2012

Physiological and Morphological Characterization of Genetically Defined Classes of Interneurons in Respiratory Rhythm and Pattern Generation in Neonatal Mice

Maria Cristina De Guzman Picardo
College of William & Mary - Arts & Sciences

Physiological and Morphological Characterization of Genetically Defined Classes of Interneurons in Respiratory Rhythm and Pattern Generation in Neonatal Mice

Maria Cristina De Guzman Picardo

Newport News, Virginia

Master of Science, College of William and Mary, 2010
Bachelor of Science, University of the Philippines, 1998

A Dissertation presented to the Graduate Faculty
of the College of William and Mary in Candidacy for the Degree of
Doctor of Philosophy

Department of Applied Science

The College of William and Mary
August 2012

APPROVAL PAGE

This Dissertation is submitted in partial fulfillment of
the requirements for the degree of

Doctor of Philosophy

Maria Cristina De Guzman Picardo

Approved by the Committee, July, 2012

Committee Chair
Dr. Christopher A. Del Negro
Applied Science, College of William and Mary

Dr. Hannes C. Schniepp
Applied Science, College of William and Mary

Dr. Lizabeth A. Allison
Biology, Collge of William and Mary

Dr. Margaret S. Saha
Biology, College of William and Mary

Dr. Paul A. Gray
Anatomy and Neurobiology, Washington University

COMPLIANCE PAGE

Research approved by

Institutional Animal Care and Use Committee

Protocol number(s):

IACUC-2007-07-26-6795-cadeln
IACUC-2010-07-12-6795-cadeln

Date(s) of approval:

July 26, 2008
July 26, 2009
July 30, 2010
July 30, 2011
July 30, 2012

ABSTRACT PAGE

Breathing in mammals depends on an inspiratory-related rhythm that is generated by glutamatergic neurons in the preBötzinger complex (preBötC), a specialized site of the lower brainstem. Rhythm-generating preBötC neurons are derived from a single lineage that expresses the transcription factor (TF) *Dbx1*, but the cellular mechanisms of rhythmogenesis remain incompletely understood. To elucidate these mechanisms we comparatively analyzed *Dbx1*-expressing neurons (*Dbx1*$^+$) and *Dbx1*$^-$ neurons in the preBötC in knock-in transgenic mice. Whole-cell recordings in rhythmically active newborn mouse slice preparations showed that *Dbx1*$^+$ neurons activate earlier in the respiratory cycle and discharge greater magnitude inspiratory bursts compared to *Dbx1*$^-$ neurons. Furthermore, *Dbx1*$^+$ neurons required significantly less input current to discharge spikes (rheobase) in the context of network activity. The expression of intrinsic membrane properties indicative of A-current (I_A) and hyperpolarization-activated current (I_h) was generally mutually exclusive in *Dbx1*$^+$ neurons, which may indicate rhythmogenic function. In contrast, there was no such relationship in the expression of intrinsic currents I_A and I_h in *Dbx1*$^-$ neurons. Confocal imaging and digital reconstruction of recorded neurons revealed dendritic spines on *Dbx1*$^-$ neurons, but *Dbx1*$^+$ neurons were spineless. *Dbx1*$^+$ neuron morphology was largely confined to the transverse plane whereas *Dbx1*$^-$ neurons projected dendrites to a greater extent in the parasagittal plane (rostrocaudally). A greater percentage of *Dbx1*$^+$ neurons showed contralaterally projecting axons whereas *Dbx1*$^-$ neurons showed axons projecting in the rostral direction, which were severed by transverse cutting of the slice. Our data suggest that the rhythmogenic properties of *Dbx1*$^+$ neurons include a higher level of intrinsic excitability that promotes burst generation in the context of network activity, which may be attributable to dendritic active properties that are recruited by excitatory synaptic transmission. Along with *Dbx1*, the TF *Math1* has been shown to give rise to neurons that have important respiratory functions, including a potential role in coordinating the inspiratory and expiratory phases. To evaluate this role, we performed physiological and morphological characterizations of *Math1*$^+$ neurons in transgenic mice and found that one out of six recorded *Math1*$^+$ neurons showed expiratory activity. The expiratory *Math1*$^+$ neuron appeared to be have a larger soma as well as a greater somatodendritic span in all axes (dorsal-ventral, medial-lateral and rostral-caudal) than the non-respiratory modulated *Math1*$^+$ neurons. This suggests that respiratory modulated *Math1*$^+$ neurons may be physiologically and morphologically specialized compared to non-rhythmic *Math1*$^+$ neurons. Their larger morphological span and rhythmic expiratory modulation could be indicative of a function in coordinating phasic activity between inspiratory and expiratory oscillators. Although our findings are still preliminary, the data thus far are consistent with a hypothesized respiratory network model wherein the *Math1*$^+$ neurons function in coordinating the pattern of inspiration and expiration. Identifying and characterizing hindbrain interneurons according to developmental genetic origins as well as physiological properties provides complementary information to help elucidate the cellular mechanisms underlying the generation and coordination of the respiratory rhythm.

TABLE OF CONTENTS

DEDICATION PAGE

This dissertation is dedicated to my family,
especially my mom Ena,
husband Aris, and son Arvin.

ACKNOWLEDGEMENTS

It is with immense gratitude that I acknowledge Christopher A. Del Negro, Ph.D., for persevering with me as my advisor through out the time it took me to complete this research and write the dissertation.

I consider it an honor to work with the following members of my committee, Paul A. Gray, Ph.D.; Margaret S. Saha, Ph.D.; Lizabeth A. Allison, Ph.D.; and Hannes C. Schniepp, Ph.D., who have generously given their time and expertise in reviewing this dissertation.

I acknowledge and credit the work of Krishanti Weragalaarachchi and Victoria Akins who provided assistance in the form of digital morphological reconstructions and analyses, which comprise an important part of Chapters 2 and 3 of this dissertation.

I am indebted to Margaret S. Saha, Ph.D., for allowing me to use their laboratory resources for neuroanatomy work, and to Lizabeth A. Allison, Ph.D., for sharing her molecular biology expertise and providing answers to my questions about transgenic mice.

My thanks and appreciation to my professors Gregory D. Smith, Ph.D.; Leah B. Shaw, Ph.D.; Eric L. Bradley, Ph.D.; and Walter Silva, Ph.D.; and our colleague John A. Hayes, Ph.D., who were major influences on my intellectual development in my early days as a new graduate student.

I wish to thank my many colleagues in the lab Krish, Victoria, Andrew, Wiktor and Chris for all their friendship, support and help. Special thanks go to my batchmate Snow, who has gone through these four years with me and witnessed my successes and failures.

My sincerest appreciation to all the faculty and staff in the Department of Applied Science, especially Lydia, Destiny and Rosi. My work and graduate student life would have been more difficult without their help and support.

This dissertation would not be possible without the financial support from the National Institute of Neurological Disorders and Stroke (NINDS) Ruth L. Kirchstein National Research Service Award (NRSA) Fellowship Grant 1-F31-NS071860-01.

My heartfelt thanks to my parents, sister, brother and their families, my extended family, in-laws and friends who have always supported, encouraged and believed in me.

I owe my deepest gratitude to my husband Aris, whose love, support and constant patience have taught me so much about sacrifice, discipline and compromise, and to my son Arvin, who is my great source of love, joy and relief from scholarly endeavor.

Above all, I am ever grateful to God, to whom I owe my very existence and give all the glory.

LIST OF TABLES

LIST OF FIGURES

CHAPTER 1: Transcription factors influence circuit formation in spinal cord and hindbrain development

Rhythmic behaviors such as breathing, chewing, and locomotion originate due to activity in neural circuits termed central pattern-generators (CPG) that are located in the brainstem and spinal cord (Grillner, 2006; Kiehn, 2011). Previous studies of CPGs have largely focused on invertebrate model systems due to their relative simplicity. These studies involved physiological experiments on neurons that could be defined unambiguously by anatomical location in specific ganglia (Orlovsky et al., 1999). While this approach is primarily useful in studying invertebrate systems, it has limited applicability in examining CPGs in vertebrates, in particular mammals, due to the large number of functionally distinct neurons that are mixed together in the brainstem and spinal cord. Consequently, more than two decades of physiological recordings have not revealed the cellular and ionic bases for rhythmogenesis in mammalian CPGs for key rhythmic behaviors.

A new approach for identifying cells that comprise the mammalian CPG circuits is carried out in terms of specific genetically defined classes of neurons whose roles in generating and coordinating aspects of the behaviors can be determined experimentally. Individual neurons adopt and maintain distinct morphological and physiological characteristics in part as a result of the expression of specific combinations of transcription factors (TFs). TFs control the expression of other genes and thus play a principal role in regulating patterns of development in the brain and central nervous system (CNS). The use of fluorescent reporter proteins (or non-fluorescent reporters such as ß-galactosidase encoded by *LacZ*) allows for mapping the development of these genetically defined populations. Moreover, fluorescent reporters in living specimens enable visual identification and selective physiological recording of TF-derived classes of neurons in studies that help elucidate the cellular bases for network function.

Combinatoric expression of TFs provides markers to identify specific neuronal subpopulations (Tanabe and Jessell, 1996; Gray et al., 2004; Dasen et al., 2005; Gray, 2008; Garcia-Campmany et al., 2010). In vertebrates, discrete domains of spinal progenitor cells at defined locations in the neural tube express a code of TFs, which then lead to the formation of motoneurons, interneurons, and sensory neurons (Briscoe and Ericson, 2001). These populations can first be identified at approximately embryonic day 10 (E10), and by E13, they begin to migrate toward their settling positions, which they reach before birth and where they remain postnatally. The axons and dendrites of these neurons are then specified as a result of the asymmetrical distribution of membrane components caused by the last mitotic division of the neural progenitor cells (de Anda et al., 2005), combined with the action of cytoplasmic determinants such as mRNAs and proteins, or extracellular polarizing factors (Esch et al., 1999; Jacobson et al., 2006; Arimura and Kaibuchi, 2007; Shelly et al., 2010). Both the notochord, which defines the primitive axis of the vertebrate embryo, and the floor plate, found on the ventral midline of the embryonic neural tube, express sonic hedgehog (SHH) that induces the formation and differentiation of neurons in the ventral tube (Jessell, 2000; Shirasaki and Pfaff, 2002). On the other hand, the primary signals for the induction of dorsal cell fate are members of the bone morphogenetic protein (BMP) family secreted from the roof plate (Lee and Jessell, 1999). The opposing gradients of SHH and BMP in the neural tube influence the subsequent patterns of TF expression, leading to further steps in the differentiation process of progenitor neurons (Liem et al., 2000; Wilson and Maden, 2005). Aside from divergent TF expression, progenitor domains can also differentiate into a variety of genetically distinct subpopulations due to time of birth or epigenetic mechanisms, therefore it is possible that no two neurons express the exact same genes at the same time (Masland, 2004; Sugino et al., 2006; Gray, 2008). Nevertheless, studying neurons developed from the same progenitors may still provide essential

information on shared characteristics that may help elucidate CPGs in the brainstem and spinal cord.

During spinal cord development, progenitor domains within the ventral neural tube generate distinct classes of neurons that then assemble core constituents of the spinal locomotor CPG. In the embryonic mouse, the developing neural tube can be subdivided into eleven distinct populations of spinal neurons (dI1–dI6, V0–V3, MN) located at different positions (Fig. 1A). The dI1-dI5 neurons arise from dorsal progenitor domains and are mainly involved in spinal sensory pathways (Bermingham et al., 2001; Goulding et al., 2002; Gross et al., 2002; Qian et al., 2002; Helms and Johnson, 2003). In the dorsal half of the neural tube, dI1 is located in the dorsalmost position and is followed ventrally by dI2, dI3, dI4 and dI5. On the other hand, dI6, V0-V3 and MN neurons are derived from intermediate/ventral progenitor domains and play an important role in spinal locomotor pathways (Brown, 1981; Kjaerulff and Kiehn, 1996; Goulding, 2009). dI6 is the dorsalmost domain in the ventral half of the neural tube, followed ventrally by V0, V1, V2, MN and V3. Analyses of the ventral domains, particularly the V0-V3, have helped explore the cellular bases for locomotor function (Lanuza et al., 2004; Goulding and Pfaff, 2005; Kiehn, 2006; Zhang et al., 2008; Goulding, 2009; Kiehn, 2011). These analyses employ genetic cell marking methods that allow tracing the fates of genetically defined progenitor populations, even after the progenitor cells lose expression of the gene upon differentiation into neurons (Vue et al., 2007). Knocking-out or silencing genetic populations, by expressing channels that impede neuronal activity or by blocking synaptic transmission, are also useful methods in studying the organization of locomotor CPG (Pierani et al., 2001; Lanuza et al., 2004; Gosgnach et al., 2006; Crone et al., 2008; Zhang et al., 2008; Crone et al., 2009).

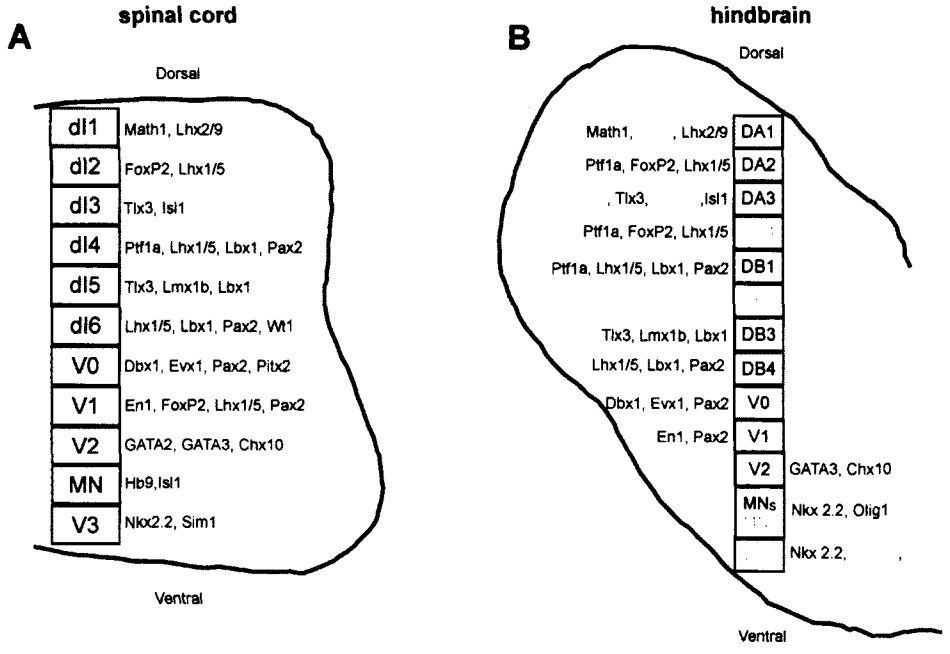

Figure 1.1 Gene expression patterns in the developing spinal cord (A) and hindbrain (B). **A**, The right half of the spinal cord showing the five dorsal (dI1-dI5) and six ventral (dI6-V3) progenitor domains (rectangular boxes) based on their relative position along the dorsoventral axis of the neural tube. To the right is a partial list of transcription factors (TFs) expressed at some point in the progenitor and post-mitotic stages of each of the domains. **B**, The left half of the hindbrain showing the seven dorsal (DA1-DB4) and six ventral (DB4-V3-L) domains (rectangular boxes) that correspond to the spinal cord domains, and some of the progenitor and post-mitotic TFs expressed. Domains and TFs in red are brainstem specific. Other TFs not included in the text are *Lhx2/9, Tlx3, Lbx1* and *Wt1*, which are expressed in the dorsal progenitor domains of the spinal cord and the brainstem(Porter et al., 1997; Birk et al., 2000; Muller et al., 2002; Cheng et al., 2004; Cheng et al., 2005; Goulding, 2009). The ventral progenitor domain MN expresses *Hb9* and *Isl1* and gives rise to motoneurons (Pfaff et al., 1996; Arber et al., 1999). Note that the intermediate/ventral domains in the spinal cord (dI6) and brainstem (DB4) are considered part of the dorsal domains in other references.

Located at the dorsal-ventral boundary of the developing neural tube, the V0 populations arise from progenitors that express *Pax2*, *Dbx1*, and *Dbx2* between E10 and E13 (Pierani et al., 1999). Postmitotic V0 neurons express the homeodomain proteins *Evx1* and *Evx2* (Burrill et al., 1997; Matise and Joyner, 1997; Pierani et al., 1999; Moran-Rivard et al., 2001). The V0 interneurons settle in the ventro-medial spinal cord and are present in all spinal segments (Pierani et al., 1999). With commissural axon projections, V0 interneurons are important in coordinating left-right alternation during locomotion (Pierani et al., 2001; Lanuza et al., 2004). V0 interneurons can be further subdivided.

The dorsally located $V0_D$ are either GABAergic or glycinergic inhibitory neurons, while the ventrally located $V0_V$ populations are glutamatergic neurons. The $V0_{C/G}$ subpopulation, hypothesized to be a subset of the $V0_V$ group, expresses the transcription factor *Pitx2*, transiently expresses *Evx1*, and is either cholinergic ($V0_C$) or glutamatergic ($V0_G$). Unlike majority of the $V0_D$ and $V0_V$, whose axons extend commissurally, the $V0_{C/G}$ populations project their axons ipsilaterally and provide excitatory input onto motoneurons (Zagoraiou et al., 2009).

Next, the V1-derived population, found more ventral in the neural tube to the V0 population, expresses the TFs *En1* and *FoxP2*. V1 progenitor cells give rise to mostly inhibitory (GABAergic or glycinergic) neurons including Renshaw and Ia inhibitory interneurons, which are core contributors to spinal locomotor control circuits (Pratt and Jordan, 1987; Sapir et al., 2004; Alvarez et al., 2005). The majority of the V1 neurons have ipsilateral projections that extend rostrally (Saueressig et al., 1999; Higashijima et al., 2004) and regulate the speed of locomotor rhythm, and in particular are required for faster gait-like patterns of fictive locomotor activity (Gosgnach et al., 2006).

The V2 population is derived from *Lhx3*-expressing progenitors, and can be divided into the V2a subpopulation that expresses the transcription factor *Chx10* (Peng et al., 2007) and the V2b subpopulation that expresses *Gata2* and *Gata3* (Ericson et al., 1997; Zhou et al., 2000; Karunaratne et al., 2002; Smith et al., 2002). V2 neurons are found throughout lamina VII of the postnatal spinal cord, extending from the central canal out toward the lateral edge of the gray matter (Dougherty and Kiehn, 2010). The majority of V2a neurons are excitatory and extend their axons ipsilaterally (Al-Mosawie et al., 2007; Lundfald et al., 2007; Peng et al., 2007). Although dispensable for rhythm generation, V2a neurons are important in driving the left-right coordinating circuit in the locomotor CPG, thus affecting the left-right synchrony during locomotion (Crone et al.,

2008; Crone et al., 2009; Zhong et al., 2010; Kiehn, 2011). In contrast, V2b neurons are almost entirely inhibitory and a small number of V2b neurons make commissural projections (Al-Mosawie et al., 2007; Lundfald et al., 2007; Peng et al., 2007), and are proposed to serve a complementary function in coordinating left-right alternation in the locomotor CPG (Kiehn, 2011).

Lastly, originating in the ventral extreme of the developing neural tube, the V3 interneurons are another population of mainly excitatory cells in the mammalian spinal cord (Zhang et al., 2008). These neurons derive from *Nkx2.2/2.9*-expressing progenitors and express the transcription factor *Sim1* postmitotically (Briscoe et al., 1999; Goulding et al., 2002). V3 neurons migrate to the dorsomedial and ventromedial regions of the spinal cord postnatally. The majority of these neurons extend their axons contralaterally and are hypothesized to be involved in ensuring a regular and symmetrical movement pattern by distributing the locomotor rhythmic output between both sides of the spinal cord (Zhang et al., 2008).

The loss of any of these cardinal classes of ventrally located populations alters, but does not stop, locomotor activity. Collectively, these results show that spinal cord CPG rhythmicity cannot be traced to any single population of interneuron yet identified by gene expression patterns or developmental origin. This may be due, in part, to the distributed nature of the spinal cord CPG circuits, which are thought to be located (at least in cats and rodents) in the ventral part of the cord throughout lumbar segments 1-6 (L1-L6) and sacral segments 1 and 2 (S1, S2), with a rostrocaudal gradient in excitability that favors rhythmogenic function concentrated between L1-L3 for rodents (Kiehn, 2006). This concept of a distributed locomotor CPG is also consistent with the previous proposal that each joint may have its own unit oscillator, rather than a single oscillatory center that drives the overall locomotor rhythm (Grillner, 2006).

The respiratory rhythmogenic circuits in the brainstem are not distributed in the anterior-posterior axis like spinal cord locomotor circuits. Rather, respiratory rhythm putatively originates in the limited borders of the preBötzinger complex (preBötC), a functionally and anatomically specialized region of the ventrolateral medulla that is necessary for breathing in rodents (Smith et al., 1991; Gray et al., 1999; Gray et al., 2001; Feldman and Del Negro, 2006; Tan et al., 2008). Specifically, the preBötC is the putative site for the origin of inspiratory rhythm, which dominates the respiratory cycle (Feldman and Del Negro, 2006; Janczewski and Feldman, 2006). The preBötC has been identified in terrestrial mammals including rats (Smith et al., 1991; Gray et al., 1999), mice (Rekling and Feldman, 1998; Bouvier et al., 2010; Gray et al., 2010), cats (Schwarzacher et al., 1995), goats (Wenninger et al., 2004), and humans (Schwarzacher et al., 2010). What also sets breathing apart is bilateral synchrony; the lack of flexor-extensor activity provides a somewhat 'simpler' rhythmic activity to scrutinize at the cellular level. Due to the alternating left-right and flexor-extensor nature of locomotion, inhibitory commissural and projection interneurons are essential components of the spinal cord CPGs. Conversely, the respiratory CPG depends exclusively on excitatory transmission (Funk et al., 1993; Wallen-Mackenzie et al., 2006), and commissural excitatory interneurons in particular (Koshiya and Smith, 1999; Bouvier et al., 2010). Inhibitory interneurons are not obligatory for rhythm generation and their interactions do not impact the frequency of respiratory rhythm *in vitro* (Feldman and Smith, 1989; Shao and Feldman, 1997; Brockhaus and Ballanyi, 1998; Ritter and Zhang, 2000; Ren et al., 2006).

Breathing-related neurons are located throughout the hindbrain in a ventral respiratory column (VRC) extending from the caudal facial motor nucleus (VII) to the phrenic motor nucleus of the cervical spinal cord (C3-C5). The preBötC lies approximately in the middle of the VRC along the anterior-posterior axis. Additionally

there are respiratory neurons in the pons and dorsal respiratory nuclei including, notably, the *nucleus tractus solitarius*, but these dorsal respiratory groups are involved in modulation of respiratory activity and sensorimotor integration (Blessing, 1997) and thus are not the principal focus of this dissertation.

Mutations in genes encoding a number of TFs in the brainstem, where over 100 different TFs are expressed, affect breathing *in vivo*, *in vitro* or both (Dubreuil et al., 2008; Gray, 2008; Bouvier et al., 2010; Gray et al., 2010; Ramanantsoa et al., 2011). In many cases, such mutations affect respiratory neurons in the VRC. As previously mentioned, there are at least 11 genetically distinct populations identified on the basis of their TF expression in the spinal cord. Most of these spinal cord populations exhibit similar patterns of TF expression in the hindbrain. The dorsal brainstem populations DA1, DA2, DA3, DB1 and DB3 correspond to the dI1, dI2 and dI3, dI4 and dI5 spinal domains, respectively. The ventral brainstem progenitor domains DB4, V0, V1 and V2 match the dI6, V0, V1 and V2 spinal domains (Fig. 1B). At least three additional populations (DA4, DB2, MN_V) of neurons have no related spinal cord homologs (Gray, 2008). Progenitors of the DA4 domain that express the TF *Ptf1a* give rise to *Lhx1/5*-expressing glutamatergic populations and are fated to populate the inferior olivary nuclei with climbing fibers that connect to GABAergic Purkinje cells in the cerebellar cortex (Yamada et al., 2007; Kim et al., 2008). The DB2 domain gives rise to glutamatergic interneurons that express *Phox2b*, *Lbx1* and *Math1*; a significant subset – but not all – of these DB2-derived neurons provide chemosensory drive for respiration (Pattyn et al., 1997; Dubreuil et al., 2000; Pattyn et al., 2000; Sieber et al., 2007; Pagliardini et al., 2008; Goridis et al., 2010). The ventralmost MN_V and V3-like (V3-L) hindbrain domains both derive from *Nkx2.2/Nkx2.9*-expressing progenitors. The MN_V domain expresses *Olig1* whereas the V3-L domain expresses *Lmx1b* and *Pet1* (Gray, 2008). These two domains differentiate into branchiomotor neurons that innervate muscles derived from

the branchial arches such as the trigeminal (V) and facial (VII) motoneurons, visceral motor neurons that innervate the sympathetic and parasympathetic ganglia, and somatic motor neurons in the hypoglossal (XII) nuclei (Briscoe et al., 1999; Pattyn et al., 2004; Gray, 2008).

The preBötC contains a heterogeneous mixture of respiratory-related neurons; which of these neurons generate the respiratory rhythm? Contemporary attempts to understand the cellular basis for respiratory rhythm generation focus on excitatory glutamatergic neurons that express the vesicular glutamate transporter 2 (Vglut2$^+$), as well as neurons that express neuropeptides and peptide receptors (Gray et al., 1999; Gray et al., 2001; Guyenet and Wang, 2001; Wang et al., 2001; Guyenet et al., 2002; Stornetta et al., 2003; McKay et al., 2005; Tan et al., 2008). Excitatory amino acid-mediated neurotransmission is essential for rhythmogenesis *in vitro* (Greer et al., 1991; Funk et al., 1993) and *in vivo*, Vglut2 null mice die because the preBötC fails to become active (Wallen-Mackenzie et al., 2006). Peptidergic neurotransmission potently modulates respiratory rhythm *in vitro* (Rekling et al., 1996a; Gray et al., 1999), and *in vivo*, ablation of neurons expressing neurokinin-1 receptor (NK1R) results in ataxic breathing while genetic silencing of somatostatin (SST) peptide-expressing neurons induces persistent apnea (Gray et al., 2001; McKay et al., 2005; Tan et al., 2008). SST2a receptors are also co-expressed with SST and NKIR in neurons within the preBötC (Gray et al., 2010). These findings signify the importance of preBötC glutamatergic neurons and preBötC neurons that express peptides and peptide receptors, notably SST, SST2a receptors and NK1R, in respiratory rhythm generation. Fortuitously, neurons with glutamatergic and peptidergic transmitter phenotypes, which also express peptide receptors, are derived from the same progenitor population. Our group and another group show that rhythm-generating neurons in the mouse preBötC are derived from the V0 population that expresses the TF Developing Brain Homeobox 1

(*Dbx1*) during embryonic development (Bouvier et al., 2010; Gray et al., 2010). *Dbx1*-null ($Dbx1^{-/-}$) mice die at birth without taking a breath; there are no inspiratory or expiratory movements *ex utero*. At the cellular level, $Dbx1^{-/-}$ mice show no evidence of a preBötC based on the lack of cellular expression of peptide markers and Vglut2 relative to other hindbrain structures and nuclei (Pierani et al., 2001; Gray et al., 2010).

To evaluate the role of *Dbx1*-derived ($Dbx1^{+}$) neurons in respiratory rhythm generation, we characterize their physiological and morphological properties using a genetic fate mapping approach. $Dbx1^{+}$ neurons are studied using heterozygous *Dbx1*-β-gal knock-in mice ($Dbx1^{LacZ/+}$) (Pierani et al., 2001) where the persistence of the beta-galactosidase (β-gal) protein can be used to fate-map neurons. This fate mapping strategy involves marking cell bodies with β-Gal that can be visualized in fixed tissues, usually after first performing physiological experiments. Another genetic fate mapping strategy, which is based on the cre-lox recombination system, is particularly useful for the present dissertation because it facilitates characterization of the properties of neurons in living slices with intact respiratory network functions. An expression cassette was constructed by Hirata and colleagues, wherein cre recombinase is fused to the tamoxifen sensitive estrogen receptor (ER^{T2}) and linked at its 5' end to an internal ribosome entry site (IRES). The IRES-$CreER^{T2}$ was inserted in the 3' untranslated region (UTR) of the *Dbx1* gene to permit inducible labeling of the $Dbx1^{+}$ cells (Hirata et al., 2009). The *cre* has the same expression patterns as that of the *Dbx1* as shown in a study on the amygdala (Hirata et al., 2009). Crossing the $Dbx1^{CreERT2}$ transgenic mice with floxed reporter mice produces *Dbx1* cells labeled with the fluorescent reporter proteins, which can be targeted in electrophysiological recordings. To facilitate identification and recording of fluorescently labeled $Dbx1^{+}$ neurons in this study, it is important to use floxed reporter mice with very bright fluorescent proteins, that resist bleaching of the fluorescent signal for the duration of the electrophysiological

experiments. Initially, we cross the *Dbx1*^{CreERT2} mice with the readily available reporter mouse expressing the enhanced yellow fluorescent protein (*Rosa26*^{EYFP}), but the fluorescent signal of the EYFP-labeled cells is weak, which makes it difficult to identify and subsequently obtain patch-clamp recordings from *Dbx1*$^{+}$ neurons. We now favor a reporter mouse with the fluorescent protein tdTomato (we refer to this strain as *Rosa26*^{tdTomato}), which, compared to the EYFP protein, gives much brighter fluorescently labeled *Dbx1*$^{+}$ neurons for electrophysiological recordings (Madisen et al., 2010).

Elucidating the rhythmogenic role of the *Dbx1*$^{+}$ neurons in the respiratory CPG requires electrophysiological characterization of their membrane properties. The preBötC can be isolated in an *in vitro* brainstem slice preparation that spontaneously generates inspiratory-related rhythmic motor output measurable via suction electrodes on the XII nerve rootlets, which contain axons for respiratory-related motoneuron cell bodies also captured in the slice. Through intracellular recordings, we demonstrate that *Dbx1*$^{+}$ neurons are inspiratory, i.e. produce bursts that coincide with the XII motor output (Gray et al., 2010). However, knowing that *Dbx1*$^{+}$ neurons are inspiratory does not, in itself, provide any insight regarding the cellular and synaptic mechanisms of rhythm generation. Therefore, we measured membrane properties to analyze synaptic integration and the factors that influence *Dbx1*$^{+}$ neuron excitability. The inspiratory drive potentials of preBötC neurons, including the *Dbx1*$^{+}$ populations, depend on excitatory synaptic input coupled to intrinsic membrane properties. In general, neurons of different classes (e.g., cortical pyramidal, Purkinje, basket, amacrine, etc...) express distinctive complements of intrinsic properties that influence their unique electrical responses to chemical or electrical synaptic inputs (Llinas, 1988). In this study, we measure basic intrinsic membrane properties of *Dbx1*$^{+}$ neurons such as input resistance, capacitance, time constant and rheobase that could be important for understanding synaptic integration and burst generation in support of respiratory rhythmogenesis. In addition,

properties such as the presence of transient outward current, i.e., A-type K^+ current (I_A), and the hyperpolarization-activated h-current (I_h), which can be identified by 'delayed excitation' and 'hyperpolarizing sag potentials' in current-clamp recordings, respectively (see Chapter 2), have been hypothesized to shape the inspiratory drive potential, i.e., the envelope of depolarization underlying an inspiratory burst (Rekling et al., 1996b; Thoby-Brisson et al., 2000; Hayes, 2007). The differences or similarities in the membrane properties of the rhythmogenic *Dbx1*$^+$ versus non-rhythmogenic *Dbx1*$^-$ preBötC neurons could help reveal the mechanisms that generate the inspiratory rhythm.

Morphological characterization is done in conjunction with electrophysiological studies to augment our understanding of the cellular properties that influence respiratory rhythm generation. We particularly focus on what morphologically can differentiate *Dbx1*$^+$ from *Dbx1*$^-$ neurons. The morphology of the neuron, which includes the soma shape and size, number of dendritic projections, length, thickness and orientation of axons and dendrites, provides clues regarding extent to which dendritic and somatic sub-sections can function as separate electrical units from the standpoint of synaptic integration and neural excitation (Mainen and Sejnowski, 1996). Prior to this study, there have not been any morphological characterizations performed for any *Dbx1*$^+$ subpopulation, neither in the spinal cord nor in the hindbrain. The morphologies of *Dbx1*$^+$ neurons recorded from physiological experiments are analyzed and reconstructed via computer. In particular, we examine the structure and branching of the dendrites, which, together with active dendritic properties, contribute to the variability in the amplitude and time course of somatic synaptic responses and define how afferent input is transduced into action potential output (Magee, 2000; Gulledge et al., 2005). We correlate the dendritic morphology with the presence and variation of voltage-gated ion conductances, as well as intrinsic membrane properties observed from electrophysiological experiments to

understand how *Dbx1*$^+$ neurons integrate, amplify or attenuate, incoming synaptic inputs and thus shed light on the mechanisms of burst generation. Hence, morphological characterization is essential for understanding the basic structure-activity relationship in *Dbx1*$^+$ neurons.

Another TF shown to play an important role in the development of respiratory network function is Mouse Atonal Homolog 1 (*Math1, Atoh1*), which is expressed in the dorsal domains of the neural tube (Fig 1.1). *Math1* is essential for the formation of distinct hindbrain glutamatergic populations (Rose et al., 2009a; Rose et al., 2009b; Ramanantsoa et al., 2011). Mutant mice lacking the *Math1* gene appear to have normal lungs, airways and peripheral nerves, yet they die shortly after birth due to compromised glutamatergic excitatory drive, which prevents the initiation of normal respiration (Rose et al., 2009b). *Math1*$^+$ neurons also project to the area of the preBötC, however, the lack of *Math1* does not seem to affect the rhythmogenic *Dbx1* neurons or the excitatory glutamatergic transmission within the preBötC (Rose et al., 2009b). This suggests that *Math1* is obligatory for the neural control and maintenance of breathing behavior, but is not necessary for generating the inspiratory rhythm (as measured *in vitro*).

Preliminary data suggest that *Math1* could be important in coordinating the rhythm and pattern of respiratory activity (Tupal et al., 2011; Tupal et al., 2012). The respiratory network is proposed to consist of two coupled oscillators: a dominant inspiratory CPG in preBötC (Smith et al., 1991; Feldman and Del Negro, 2006) and an expiratory network which can be active or quiescent as physiological conditions demand (Mellen et al., 2003; Onimaru and Homma, 2003; Janczewski and Feldman, 2006; Abbott et al., 2011; Pagliardini et al., 2011). Inspiratory and expiratory outputs *in vitro* – generated by C4 innervation of the diaphragm and by L1 innervation of the abdominal muscles, respectively – are coupled, with a consistent temporal delay. *Math1*$^+$ neurons could be

required for this normal temporal lag between the inspiratory and expiratory activities (Tupal et al., 2011; Tupal et al., 2012). Unlike *Dbx1*$^+$ neurons, which are important for the expression of both inspiratory and expiratory behaviors (Gray et al., 2010) in perinatal rodents, *Math1*$^+$ neurons are not required for either inspiration or expiration *in vitro,* but could play a role in coordinating the rhythm and pattern of respiratory activity (Tupal et al., 2012).

In this dissertation, we investigate the role of genetically identified subpopulations of brainstem interneurons in respiratory rhythm generation, a key physiological function of the brain. The respiratory CPG is a particularly good model system to study because its constituent rhythmogenic neurons (in the preBötC) are known, and known to derive from the same genetic lineage (*Dbx1*) contained within the preBötC, while the network output is also measurable *in vitro.* By adjusting the borders of the preBötC-containing slice preparation we could also capture and examine other respiratory populations, including *Math1*$^+$ neurons (Chapter 3). Using transgenic reporter mice to aid in neuron identification, we characterize the physiological properties of *Dbx1*$^+$ and *Math1*$^+$ neurons in the preBötC and rostral regions of the VRC and measure their intrinsic membrane properties, which could help elucidate their respective roles in generating and coordinating the respiratory rhythm. The morphological characterization of *Dbx1*$^+$ and *Math1*$^+$ neurons may reveal unique principles of synaptic-dendritic integration in a rhythm-generating and coordinating network and thus provide new insights on the cellular bases of CPG function in mammals.

CHAPTER 2. Cellular and ionic mechanisms underlying rhythmogenic function of *Dbx1*-derived neurons

2.1 INTRODUCTION

The preBötzinger complex (preBötC) of the ventrolateral medulla contains the neurons that generate the inspiratory phase of the respiratory rhythm (Smith et al., 1991; Feldman and Del Negro, 2006; Janczewski and Feldman, 2006). Rhythm generation depends on glutamatergic neurons, as well as neurons that express neuropeptides and peptide receptors (Gray et al., 1999; Gray et al., 2001; Wallen-Mackenzie et al., 2006; Tan et al., 2008). Interestingly, neurons with glutamatergic and peptidergic transmitter phenotypes, that also express peptide receptors, form a superset of neurons from the same lineage. In the mouse embryo, the homeobox gene *Dbx1* controls the fate of some glutamatergic commissural interneurons in the hindbrain, including rhythm-generating preBötC neurons (Bouvier et al., 2010; Gray et al., 2010). In the absence of *Dbx1*, the preBötC does not form and mouse pups die at birth without taking a breath or making any respiratory movements, whatsoever (Pierani et al., 2001; Bouvier et al., 2010; Gray et al., 2010). We hypothesize that the intrinsic and morphological features that differentiate *Dbx1*-derived (*Dbx1*$^{+}$) neurons from non-*Dbx1*-derived (*Dbx1*$^{-}$) neurons may help elucidate the cellular mechanisms of respiratory rhythmogenesis in the preBötC.

Brainstem slices containing the preBötC spontaneously generate inspiratory motor patterns *in vitro* that can be monitored via the hypoglossal (XII) cranial nerve. Previous studies have investigated the membrane properties implicated in rhythm generation, although without regard to the gene expression patterns or transmitter phenotype of the preBötC neurons studied. During a respiratory cycle *in vitro* that lasts 2-4 s on average, putatively rhythmogenic neurons are the earliest to activate, depolarizing and starting to discharge spikes approximately 400 ms prior to the

inspiratory phase marked by XII motor output (Rekling et al., 1996b; Thoby-Brisson and Ramirez, 2001). The presence of a transient outward current, i.e., A-current (I_A), and the lack of a hyperpolarization-activated mixed cationic current, i.e., h-current (I_h), have also been hypothesized to influence inspiratory burst generation by promoting orderly recruitment of constituent rhythmogenic neurons and preventing spurious discharge (Rekling et al., 1996b; Hayes and Del Negro, 2007). Neurons distributed throughout the ventral respiratory brainstem networks, including the preBötC, express persistent Na^+ current (I_{NaP}), which gives rise to voltage-dependent membrane behaviors that are hypothesized to influence rhythmogenesis as well (Koshiya and Smith, 1999; Del Negro et al., 2002b; Ptak et al., 2005; Koizumi and Smith, 2008), but see (Del Negro et al., 2002a; Del Negro et al., 2005; Pace et al., 2007b). Finally, since 2001, it has been recognized that inspiratory bursts in preBötC neurons also involve the Ca^{2+}-activated non-specific cation current (I_{CAN}), which gives rise to large magnitude drive potentials often associated with intra-burst depolarization block of spiking. I_{CAN} has been hypothesized to be rhythmogenic (Thoby-Brisson and Ramirez, 2001; Pena et al., 2004; Crowder et al., 2007; Pace et al., 2007a; Rubin et al., 2009).

Here, we analyze the expression of the membrane properties described above in the context of new knowledge regarding the genetic source of rhythm-generating preBötC neurons. Since *Dbx1* gives rise to glutamatergic as well as peptidergic and peptide receptor-expressing rhythmogenic neurons in the preBötC, the differences between *Dbx1*$^+$ and *Dbx1*$^-$ neurons may help reveal the cellular and ionic bases for respiratory rhythmogenesis.

2.2 MATERIALS AND METHODS

The following protocols were approved by the Institutional Animal Care and Use Committee at The College of William & Mary. We used transgenic mice that express Cre

recombinase fused to the tamoxifen-sensitive estrogen receptor *Dbx1*$^{+/CreERT2}$ (Hirata et al., 2009); floxed reporter mice with inducible expression of the red fluorescent protein variant tdTomato Gt(ROSA)26Sor locus1 (*Rosa26*^{tdTomato}, Jax No. 007905) (Madisen et al., 2010); and floxed *Rosa26*^{EYFP} reporter mice with inducible expression of enhanced yellow fluorescent protein (EYFP, Jax No. 005130). Both the *Dbx1*$^{+/CreERT2}$ and *Rosa26*^{EYFP} strains were bred in-house using a CD-1 background strain. The *Rosa26*^{tdTomato} was maintained as a homozygous line with C57BL/6J background. We verified animal genotype via real-time polymerase chain reaction (PCR) using primers specific for *Cre*, *EYFP* and *tdRFP* (Transnetyx, Cordova, TN).

Neonatal mice (n = 83) were obtained from timed matings of *Dbx1*$^{+/CreERT2}$ with either *Rosa26*^{tdTomato} (n = 69) or *Rosa26*^{EYFP} reporter mice (n = 14). We visually inspected vaginal plugs to confirm successful mating and induced *Cre* recombination by administering tamoxifen to *Dbx1*$^{+/CreERT2}$ dams at embryonic day 10.5 (E10.5). If no vaginal plug was detected after four days, but the female was judged pregnant by gain of mass and visual signs of distention, then we utilized a "48-hour rule" where we counted 48 hours from the start of mating and designated that as E0. In this case, tamoxifen induction of the *Cre* recombinase falls within E9.5-E12.5, during which time *Dbx1* is expressed in hindbrain (Pierani et al., 2001; Hirata et al., 2009; Gray et al., 2010). Tamoxifen (T5648, Sigma Aldrich, St. Louis, MO) was dissolved at a concentration of 10 mg/ml in corn oil and administered by oral gavage to pregnant dams at a concentration of 1 mg per 40 g of body mass.

We anesthetized and then dissected neonatal *Dbx1*$^{+/CreERT2}$;*Rosa26*^{tdTomato} and *Dbx1*$^{+/CreERT2}$; *Rosa26*^{EYFP} mice at postnatal day 0 to 5 (P0-5) in standard artificial cerebrospinal fluid (ACSF) containing (in mM): 124 NaCl, 3 KCl, 1.5 $CaCl_2$, 1 $MgSO_4$, 25 $NaHCO_3$, 0.5 NaH_2PO_4, and 30 dextrose, equilibrated with 95% O_2 and 5% CO_2 (pH

7.4). Transverse 550-μm-thick brainstem slices with the preBötC exposed at the rostral face were obtained using a vibrating microtome. Slices were perfused with ACSF at 26-28 °C in a recording chamber on a fixed-stage Zeiss Axioskop (Thornwood, NY) with infrared-enhanced differential interference contrast (IR-DIC) imaging and epifluorescence, which enables visual identification and selective recording of target neurons.

Electrophysiology

Rhythmic respiratory-related motor output was recorded from the XII nerve rootlets, which were captured with the preBötC in transverse slices, using suction electrodes and a differential amplifier. Amplifier gain was set at 2000 and the bandpass filter was set at 300-1000 Hz (Dagan Instruments, Minneapolis, MN). The XII discharge was full-wave rectified and smoothed for display. On-cell and whole-cell patch-clamp recordings were obtained using patch pipettes with resistance of 4-6 MΩ and a Dagan IX2-700 current-clamp amplifier. IR-DIC imaging was used to target patch pipettes after fluorescent identification of *Dbx1*$^{+}$ neurons. All recordings were digitally acquired at 10 kHz using a PowerLab 16-bit A/D converter after 1 kHz low-pass filtering (AD Instruments, Colorado Springs, CO).

The patch solution contained (in mM): 140 K-Gluconate, 10 HEPES, 5 NaCl, 1 $MgCl_2$, 0.1 EGTA, 2 Mg-ATP and 0.3 Na(3)-GTP and 2 mg/ml biocytin (B4261, Sigma Aldrich). We added 50 μM of an Alexa hydrazide dye to the patch solution for fluorescent visualization of the neurons recorded in the whole-cell configuration. Alexa 568 (A10436, Invitrogen, Carlsbad, CA) was used in *Rosa26*^{EYFP}-labeled neurons and Alexa 488 (A10437, Invitrogen) was used in *Rosa26*^{tdTomato}-labeled neurons.

Current-clamp protocols were performed first in standard ACSF, and then in the presence of a cocktail of ionotropic receptor antagonists, hereafter called 'blockers' (5

μM picrotoxin, 5 μM strychnine, 10 μM CNQX, and 20 μM DL-AP5) or in a modified low Ca^{2+}/high Mg^{2+}ACSF, hereafter called 'low Ca^{2+}'. The low Ca^{2+} ACSF contained 0.5 mM Ca^{2+} and 2 mM $MgSO_4$. Equimolar substitution of Mg^{2+} for Ca^{2+} ensured that the total concentration of divalent cations remained fixed. We used standard ACSF to record membrane properties of *Dbx1*$^{+}$ neurons in conditions where the respiratory network functions *in vitro* and the synaptic and intrinsic activity can be measured in the context of respiratory rhythm. Then, we added blockers to stop the rhythm and thus measure intrinsic membrane properties in the absence of ionotropic excitatory post synaptic potentials (EPSPs) and inhibitory post synaptic potentials (IPSPs). However, metabotropic receptor-mediated synaptic transmission may still persist in the presence of blockers. Therefore we used the low Ca^{2+} ACSF to attain a more complete synaptic isolation of *Dbx1*$^{+}$ neurons and re-measure intrinsic membrane properties, albeit with the caveat of affecting Ca^{2+}-dependent K^{+} currents (Onimaru et al., 2003; Zavala-Tecuapetla et al., 2008). Nevertheless, low Ca^{2+} ACSF does not directly affect Na^{+}-dependent outward currents in preBötC neurons (Del Negro et al., 2009; Krey et al., 2010).

We analyzed inspiratory drive potentials using the *peak parameters* plugin in Chart v. 7.0 software (AD Instruments). Amplitude, area, and half width (i.e., burst duration at the 50% amplitude) were measured by digitally smoothing the traces to minimize spikes but preserve the underlying envelope of depolarization of the inspiratory drive potential (Pace et al., 2007b). Inspiratory drive latency, i.e., burst latency, quantifies the time interval during which a neuron receives temporally summating excitatory synaptic input and may begin to depolarize and discharge spikes, prior to the onset of the XII motor output, which defines the onset of the inspiratory phase *in vitro*. We measured the time interval from the point of first depolarization due to summating EPSPs above baseline membrane potential to the maximum slope of the XII output. To

determine the burst latency for any given preBötC neuron we averaged this interval from at least 5 consecutive cycles.

The membrane time constant (tau_M) was fitted by regression to an exponential decay function based on the membrane voltage response to a 500 ms hyperpolarizing current pulse from a baseline membrane potential of -60 mV. To obtain input resistance (R_N), we applied 1 s current steps from -60 mV in a 10-step sequence. We plotted the resulting voltage-current relationship (VI) and measured its slope in the linear region between (approximately) -95 and -55 mV. The whole-cell capacitance (C_M) was calculated using R_N and tau_M. To measure the rheobase at a baseline of -60 mV ($rheobase_{-60}$), we applied 12 ms current pulses and manually adjusted the step-current magnitude until it evoked a single spike on the termination of the current pulse at least 50% of the time.

We tested for membrane properties indicative of the transient outward current I_A (Rekling et al., 1996b; Hayes and Del Negro, 2007). We applied supra-threshold 500-ms depolarizing current pulses from baseline membrane potentials of approximately -80 mV and -50 mV. I_A caused a delay of 100-250 ms in spiking activity when the depolarizing current pulse was applied from a holding potential of -80 mV, but no delay in the onset of spiking activity from a holding potential of -50 mV.

We tested for I_h, a mixed cationic current activated by hyperpolarization. We applied 500-ms duration hyperpolarizing current pulses from a holding potential of -55 mV. I_h caused a voltage-dependent 'sag' response, wherein the membrane potential trajectory depolarizes back toward the holding potential during the step command.

We compared each parameter measured in *Dbx1*$^+$ and *Dbx1*$^-$ neurons at postnatal ages P0-5. Significance was assessed using a two-way ANOVA for data with multiple independent variables. The *F* values from the ANOVAs were reported with the

degrees of freedom in parentheses (between groups, within groups). For data with binary classification, we used the Fisher exact test, which is a type of Chi-square test used when a particular category has five or fewer samples. Significance was set at a minimum of $p < 0.05$.

Morphological reconstruction

Slices containing biocytin-loaded neurons were fixed in 4% paraformaldehyde in 0.1 M Na-phosphate buffer for at least 16 hours at 4°C. Slices were washed 3 times for 15 minutes each in PBS + 1% Triton X-100 and then blocked in 10% heat-inactivated fetal bovine sera (F4135, Sigma Aldrich) for 45 minutes. Finally, the slices were incubated in FITC-conjugated extravidin (E2761, Sigma Aldrich) for 2-4 hours, rinsed with PBS and coverslipped in Vectashield (H-1500, Vector Laboratories, Burlingame, CA). We visualized recorded neurons using a laser-scanning confocal microscope (Zeiss LSM 510). Images were contrast enhanced and pseudocolored using the free ImageJ software (National Institutes of Health, Bethesda, MD), and then digitally reconstructed using the freeware Neuromantic reconstruction tool (Myatt et al., 2012). The 3-D digital reconstructions functioned as tree-like digital objects that we further analyzed using the freeware L-measure (Scorcioni et al., 2008). We compared *Dbx1*$^{+}$ and *Dbx1*$^{-}$ neuron morphologies according to 39 different measurements and used two-sample unequal variance t-tests to compare morphological features between *Dbx1*$^{+}$ and *Dbx1*$^{-}$ neurons with significance set to a minimum $p < 0.05$.

2.3 RESULTS

Rhythmic properties of Dbx1^{+} and Dbx1^{-} preBötC neurons

To study *Dbx1*$^{+}$ neurons, we used brainstem slice preparations from neonatal *Dbx1*$^{+/CreERT2}$;*Rosa26*^{tdTomato} (n = 69) and *Dbx1*$^{+/CreERT2}$;*Rosa26*^{EYFP} (n = 14) mice. We

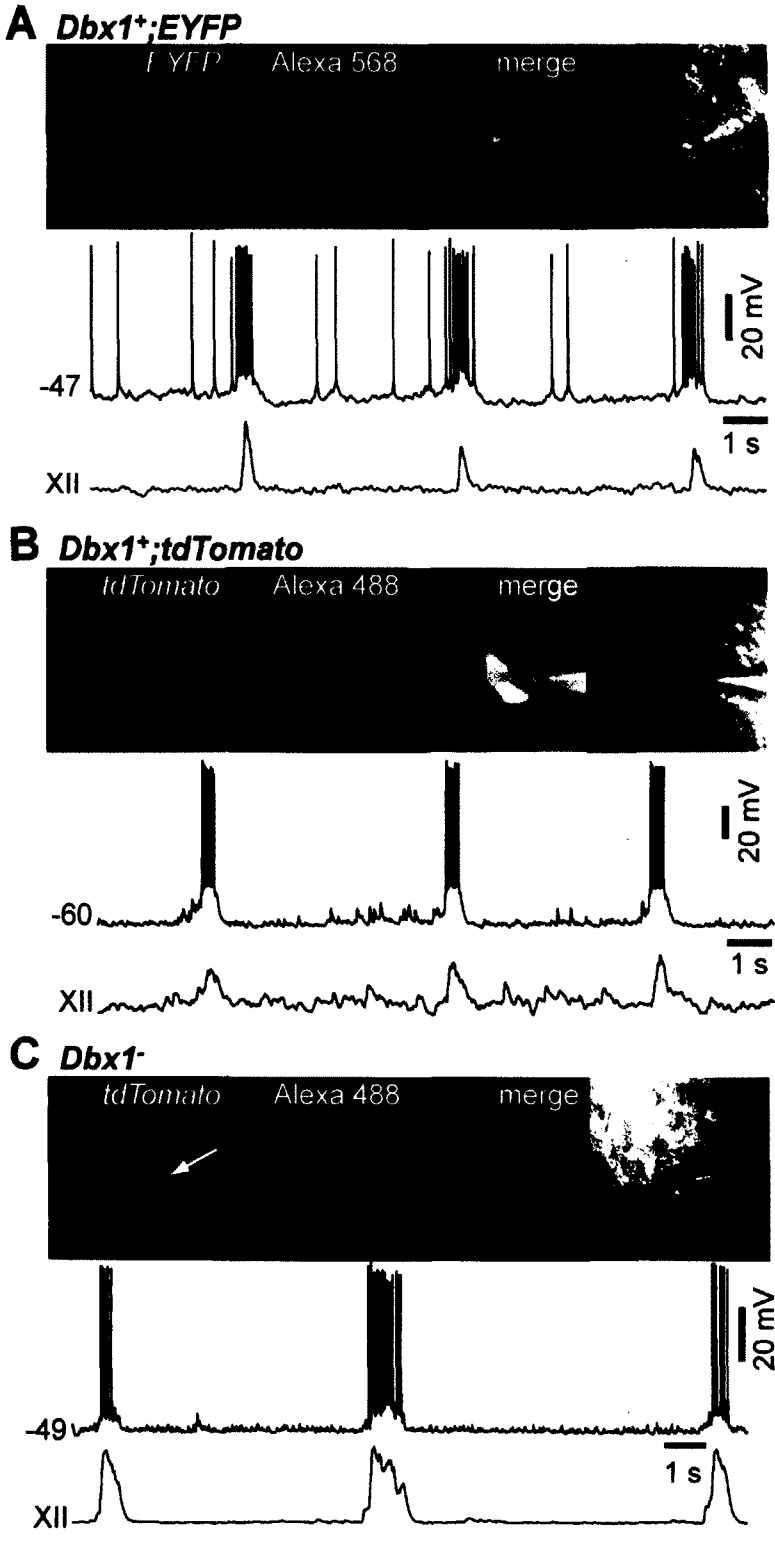

Figure 2.1 *Dbx1*$^{+}$ (A and B) and *Dbx1*$^{-}$ (C) inspiratory neurons within the preBötC of *Dbx1*$^{+/CreERT2}$; *Rosa26*^{EYFP} (A) or *Dbx1*$^{+/CreERT2}$; *Rosa26*^{tdTomato} (B and C) slice preparations. **A**, EYFP-labeled *Dbx1*$^{+}$ neuron, Alexa 568-filled, merged fluorescence, and IR-DIC images with whole-cell recording (upper) and integrated XII output (lower). **B**, tdTomato-labeled *Dbx1*$^{+}$ neuron in a *Dbx1*$^{+/CreERT2}$; *Rosa26*^{tdTomato} slice, Alexa 488-filled, merged fluorescence, and IR-DIC images with whole-cell recording (upper) and XII output (lower) **C**, unlabeled *Dbx1*$^{-}$ neuron (white arrow), Alexa 488-filled, merged fluorescence, and IR-DIC images with whole-cell recording (upper) and XII output (lower).

visually selected and recorded fluorescent *Dbx1*$^{+}$ neurons (n = 106) and non-fluorescent *Dbx1*$^{-}$ neurons (n = 42) in the preBötC, which were dialyzed with fluorescent dye to

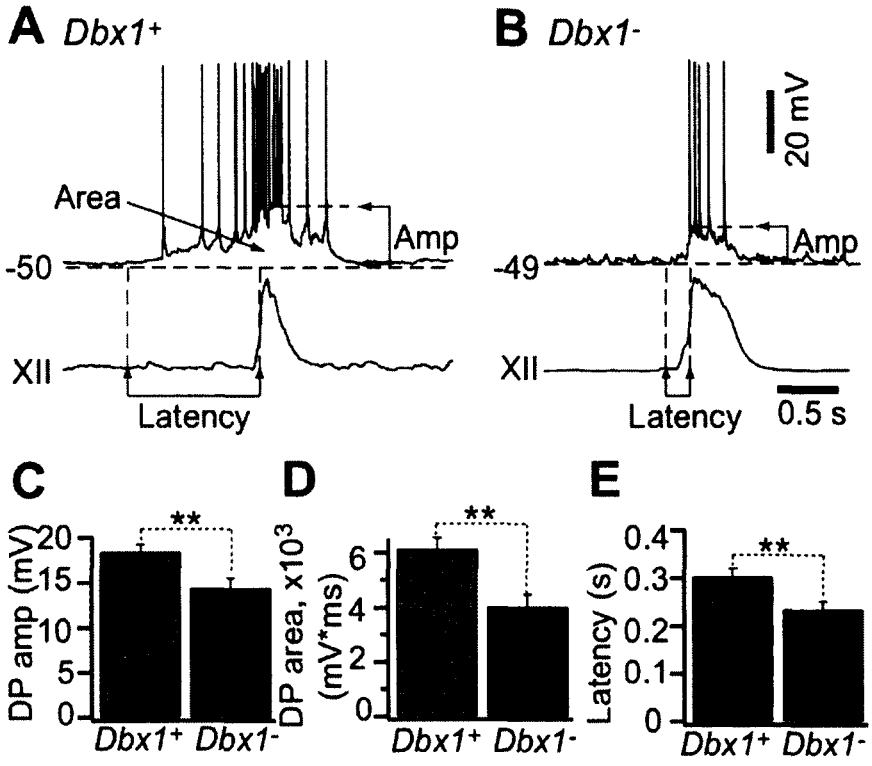

Figure 2.2 Rhythmic properties of *Dbx1*$^+$ and *Dbx1*$^-$ neurons. **A** and **B**, single inspiratory burst in a *Dbx1*$^+$ (A) and *Dbx1*$^-$ (B) neuron and the corresponding XII output (lower). Horizontal dashed lines indicate the baseline membrane potential and the amplitude of the depolarization envelope in the burst. Vertical dashed lines indicate the onsets of the inspiratory burst and the XII output, the time interval denotes latency. **C-E**. Bar charts showing the mean drive potential amplitude (C), drive potential area (D) and latency (E) of *Dbx1*$^+$ and *Dbx1*$^-$ neurons. Statistical significance indicated by ** ($p < 0.01$).

confirm the recording of the intended neuron in each case (Fig. 2.1 A-C). Inspiratory neurons were identified by depolarizing drive potentials occurring synchronously with the XII output. We measured the magnitude of the inspiratory drive potential and the inspiratory drive latency (or burst latency), which quantifies pre-inspiratory activity prior to XII output (Methods). Figure 2.1 displays the rhythmic behavior of *Dbx1*$^+$ neurons from EYFP (A) and tdTomato (B) reporter strains, and a *Dbx1*$^-$ neuron from the tdTomato strain (C), which suggests differences in drive potential characteristics and burst latency. From a baseline membrane potential of -47 mV, the *Dbx1*$^+$ neuron is active during the inter-inspiratory burst interval, including during the pre-inspiratory phase ~1 s prior to XII output. Inspiratory bursts all exceed 10 mV in amplitude in this *Dbx1*$^+$ neuron, and there

is some voltage-dependent spike inactivation (i.e., depolarization block) during the inspiratory burst (Fig. 2.1A). In contrast, the *Dbx1*$^{-}$ neuron, at a baseline of -49 mV shows a flat voltage trajectory during the inter-inspiratory burst interval, becomes active immediately prior to XII output, and its inspiratory bursts rarely exceed 10 mV (Fig. 2.1C). Even when a *Dbx1*$^{+}$ neuron is held at a hyperpolarized baseline membrane potential (-60 mV) using DC bias, summating synaptic activity is evident during the pre-inspiratory phase several hundred ms prior to XII output. In this case, the lower baseline membrane potential augments the driving force and the amplitude of the inspiratory drive potential exceeds 20 mV (Fig. 2.1B). Figure 2.2A and B illustrate the measurement of the drive potential characteristics and burst latency from a baseline of approximately -50 mV, with XII output, in a *Dbx1*$^{+}$ and a *Dbx1*$^{-}$ neuron. Because long burst latency (e.g., Fig. 2.2A) amplifies the drive potential area, we additionally assessed drive potential amplitude, which is insensitive to pre-inspiratory timing.

We measured *Dbx1*$^{+}$ and *Dbx1*$^{-}$ neurons at P0-5 to determine whether early postnatal development affects rhythmic properties. We used a two-way repeated measures ANOVA to compare the effect of age on the drive potential characteristics and burst latency between the two groups. There was no significant main effect of age on the drive potential amplitude ($F_{[5,100]} = 1.6$, $p > 0.05$), drive potential area ($F_{[5,100]} = 0.6$, $p > 0.05$), or burst latency ($F_{[5,83]} = 2.2$, $p > 0.05$), so we pooled the data for all postnatal ages (Fig. 2.2 C-E).

The main effect of group on the drive amplitude was significant ($F_{[1,100]} = 9.4$, $p < 0.01$). *Dbx1*$^{+}$ neurons showed larger drive potential amplitude (18.5 ± 0.8 mV, n = 82) compared to *Dbx1*$^{-}$ neurons (14.4 ± 1.1 mV, n = 33). There was also a significant main effect of group on drive potential area ($F_{[1,100]} = 10.6$, $p < 0.01$), where *Dbx1*$^{+}$ neurons showed larger drive potential area (6168 ± 385 mV*ms, n = 82) compared to *Dbx1*$^{-}$

neurons (4036 ± 438 mV*ms, n = 33). Drive latency was significantly different between the two groups too (F [1,83] = 7.6, $p < 0.01$), where *Dbx1*$^{+}$ neurons activated earlier (308 ± 16 ms, n = 70) compared to the *Dbx1*$^{-}$ neurons (236 ± 15 ms, n = 28).

Intrinsic membrane properties

We measured tau_M, R_N, C_M, and rheobase$_{-60}$ in standard 9 mM K^+ ACSF in the context of respiratory network activity, and then after silencing the network using a 3 mM K^+ ACSF containing a cocktail of ionotropic receptor antagonists (i.e., blockers) or low

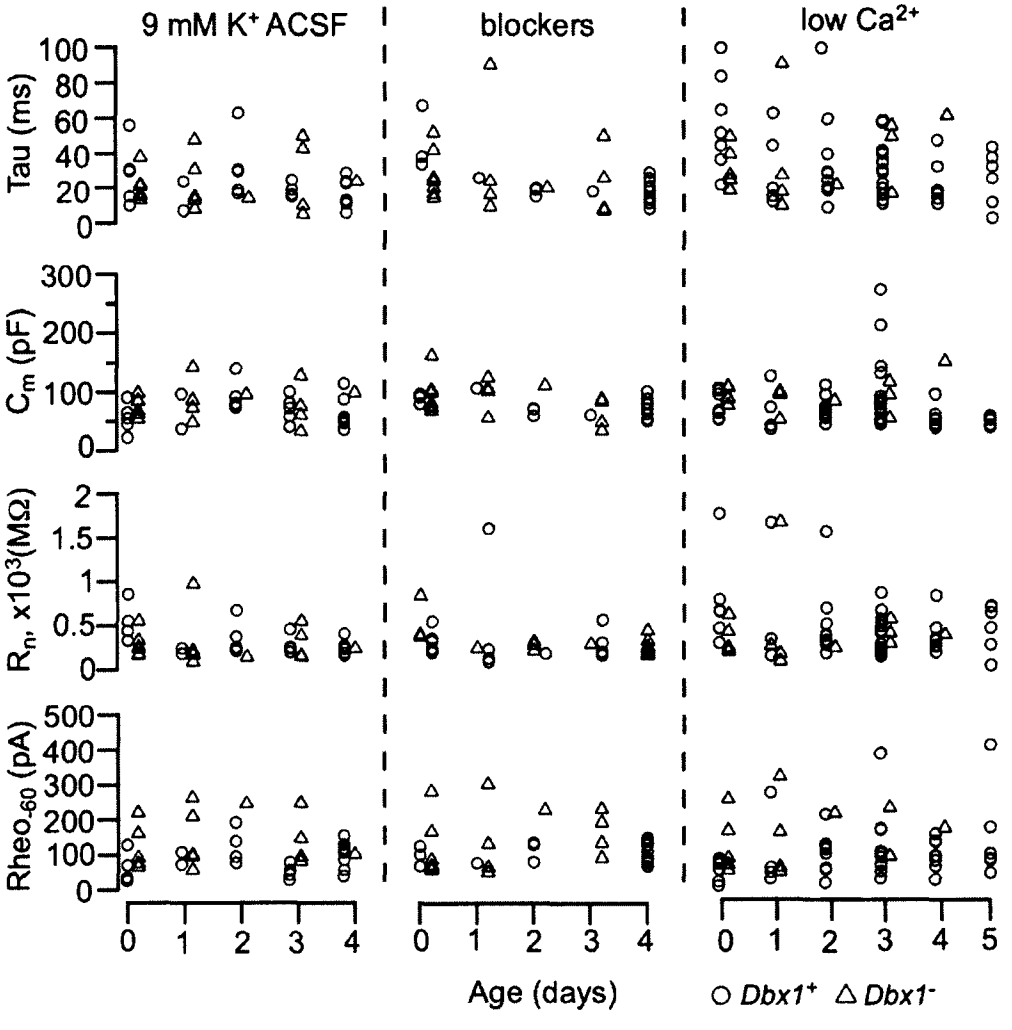

Figure 2.3 Intrinsic properties of *Dbx1*$^{+}$ and *Dbx1*$^{-}$ neurons at the different postnatal ages.

Table 2.1 Intrinsic properties of *Dbx1*$^+$ and *Dbx1*$^-$ neurons in different conditions. Statistical significance indicated by * ($p < 0.05$).

9mM K^+ ACSF	*Dbx1*$^+$	mean ± SEM	23 ± 3	340 ± 34	69 ± 5	87 ± 8*
		n	26	27	26	26
	Dbx1$^-$	mean ± SEM	23 ± 3	295 ± 54	82 ± 7	138 ± 18*
		n	17	17	17	16
blockers	*Dbx1*$^+$	mean ± SEM	24 ± 3	308 ± 38	75 ± 4	101 ± 7
		n	17	17	17	16
	Dbx1$^-$	mean ± SEM	28 ± 5	346 ± 90	88 ± 8	134 ± 21
		n	16	16	16	16
low Ca^{2+}	*Dbx1*$^+$	mean ± SEM	33 ± 3	499 ± 50	76 ± 6	107 ± 12
		n	54	51	51	46
	Dbx1$^-$	mean ± SEM	37 ± 6	428 ± 105	95 ± 7	146 ± 23
		n	14	14	14	14

Ca^{2+} ACSF. In each condition, we compared tau_M, R_N, and C_M measurements between the *Dbx1*$^+$ and *Dbx1*$^-$ neurons and at the different ages (Fig. 2.3 and Table 2.1).

Results of a two-way ANOVA revealed that there was no significant main effect of age or group on the membrane properties tau_M, R_N, or C_M over all conditions ($p > 0.05$) so we pooled the data for all postnatal ages (Table 2.1). In 9 mM K^+ ACSF, tau_M

measured 23 ± 3 ms in both *Dbx1*$^+$ (n = 26) and *Dbx1*$^-$ (n = 17) neurons (F [1,32] = 0.02, p > 0.05). R_N measured 340 ± 34 MΩ (n = 27) for *Dbx1*$^+$ and 295 ± 54 MΩ (n = 17) for *Dbx1*$^-$ neurons (F [1,33] = 0.3, p > 0.05). In *Dbx1*$^+$ neurons C_M measured 69 ± 5 pF (n = 26) and in *Dbx1*$^-$ neurons C_m measured 82 ± 7 pF (n = 17) (F [1,32] = 2.0, p > 0.05).

The two-way ANOVA revealed no main effect of age or group on the rheobase$_{-60}$ measured in blockers and low Ca^{2+}. However, there was a significant main effect of group, but not age, for rheobase$_{-60}$ in 9 mM K^+ ACSF. *Dbx1*$^+$ neurons had a lower rheobase$_{-60}$ (87 ± 8 pA, n = 26) compared to *Dbx1*$^-$ neurons (138 pA ± 18, n = 16) (F [1,27] = 7.3, p < 0.05) (Fig. 2.3 [lower left panel] and Table 2.1). These data indicate that spike threshold is lower for *Dbx1*$^+$ neurons in the context of network activity, but not when synaptically isolated using blockers or low Ca^{2+} ACSF.

Depolarization block during inspiratory bursts

We measured indirectly the influence of I_{CAN}, which promotes large inspiratory drive potentials and often causes depolarization block during inspiratory bursts (Rubin et

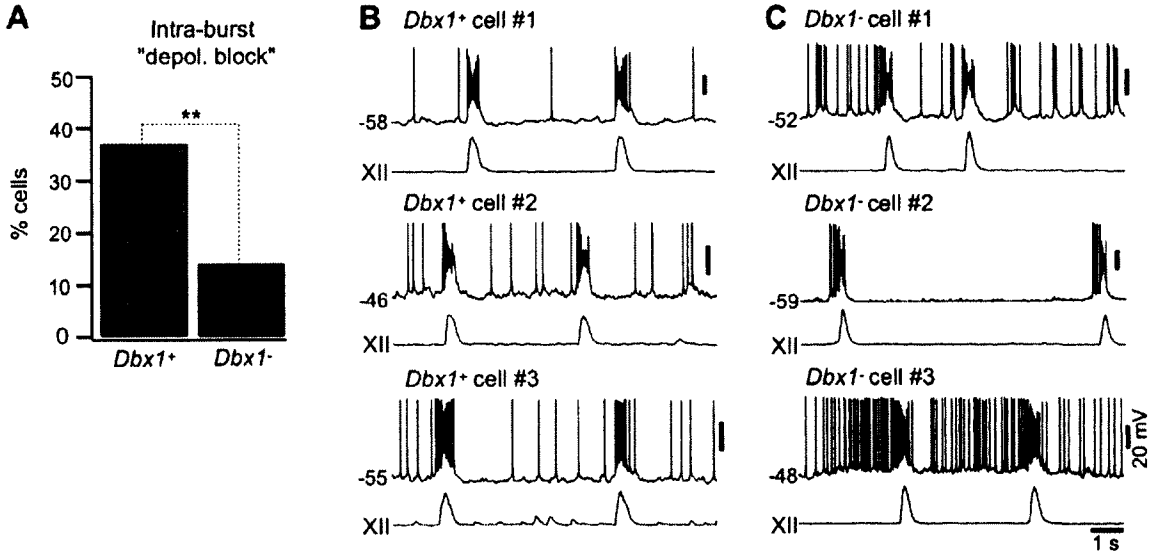

Figure 2.4 Intra-burst depolarization block in *Dbx1*$^+$ and *Dbx1*$^-$ neurons. **A**, percentage of *Dbx1*$^+$ and *Dbx1*$^-$ neurons exhibiting intra-burst depolarization. **B** and **C**, three examples of *Dbx1*$^+$ (B) and *Dbx1*$^-$ (C) neurons exhibiting depolarization block during an inspiratory burst. Vertical scale bars are all 20 mV. **Significance at p<0.01.

al., 2009; Dunmyre et al., 2011). Three different *Dbx1*$^+$ (Fig. 2.4B) and *Dbx1*$^-$ (Fig. 2.4C) neurons showing depolarization block are displayed to emphasize that this phenotype was similarly expressed in both groups. The drive potential amplitude exceeded 15 mV in *Dbx1*$^+$ and *Dbx1*$^-$ neurons with depolarization block (n=34 out of 37 total). These data suggest that both groups express I_{CAN}. However, depolarization block was more common in *Dbx1*$^+$ neurons. Thirty-one out of 91 (34%) *Dbx1*$^+$ neurons and six out of 42 *Dbx1*$^-$ neurons (14%) exhibited depolarization block in more than half of their inspiratory burst cycles, which was a statistically significant difference (Fig. 2.4A, Fisher Exact Test, $p < 0.01$).

Voltage-dependent bursting properties

We performed tests for voltage-dependent bursting properties attributable to co-expression of I_{NaP} and non-gated leak K^+ current ($I_{K\text{-}Leak}$) in the appropriate ratio (Del Negro et al., 2002b; Koizumi and Smith, 2008). Example traces show inspiratory and 'ectopic' bursts of *Dbx1*$^+$ (Fig. 2.5A) and *Dbx1*$^-$ neurons (Fig. 2.5B). Ectopic bursts that occur between inspiratory cycles of XII output, when the baseline membrane potential is

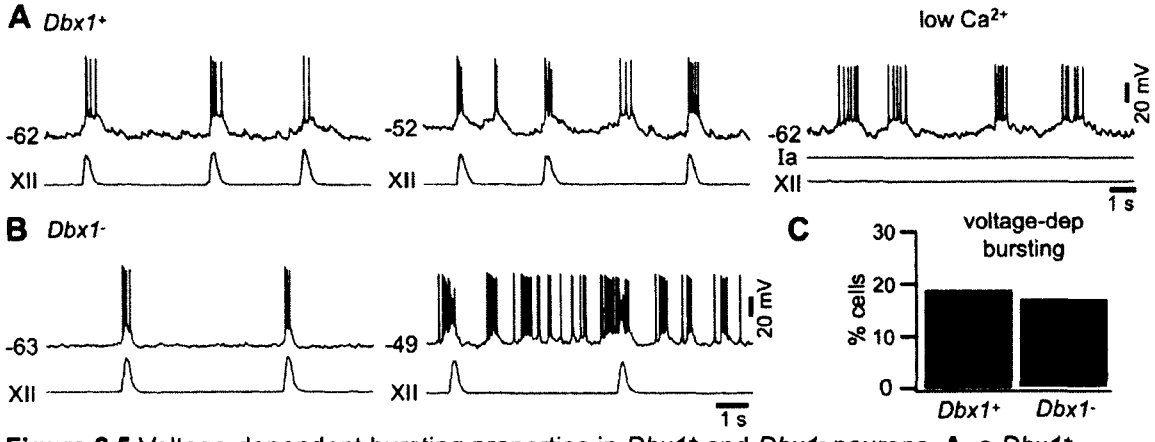

Figure 2.5 Voltage-dependent bursting properties in *Dbx1*$^+$ and *Dbx1*$^-$ neurons. **A**, a *Dbx1*$^+$ neuron showing inspiratory bursts at a baseline membrane potential of -62 mV (left), ectopic voltage-dependent bursts at a more depolarized membrane potential of -52 mV (center), and in low Ca^{2+} conditions (right). **B**, inspiratory bursts and XII output in a *Dbx1*$^-$ neuron (left) and ectopic voltage-dependent bursts at more depolarized membrane potential (right). **C**, percentage of voltage-dependent bursters in the *Dbx1*$^+$ and *Dbx1*$^-$ populations.

biased to the activation threshold of I_{NaP} (approximately -55 mV), are a reliable indicator of voltage-dependent bursting properties (Smith et al., 1991; Thoby-Brisson and Ramirez, 2001; Del Negro et al., 2002a; Del Negro et al., 2005). At baseline voltages below its activation threshold, I_{NaP} remains deactivated and ectopic bursts do not occur. Seventeen out of 91 (19%) *Dbx1*$^+$ neurons and seven out of 42 *Dbx1*$^-$ neurons (17%) exhibited ectopic bursting at membrane potentials above -55 mV, whereas burst activity for both groups was confined to the inspiratory cycles at membrane potentials less than -60 mV (Fig. 2.5C). We confirmed the voltage-dependent bursting properties by synaptically isolating 12 *Dbx1*$^+$ neurons that showed ectopic bursts. All continued bursting after application of blockers or low Ca^{2+} ACSF (Fig. 2.5A, right). The relative expression of voltage-dependent bursting activity in *Dbx1*$^+$ versus *Dbx1*$^-$ neurons was not significantly different (Fisher Exact Test, p = 1).

Relative expression of delayed excitation and 'sag' potentials

It has been proposed that preBötC neurons that express I_A, but lack I_h, are of primary importance for rhythmogenesis (Rekling et al., 1996b; Gray et al., 1999; Hayes and Del Negro, 2007). These peptide-sensitive neurons were dubbed 'type-1' to indicate their putative importance. Neurons that express I_h but not I_A, and were shown to be less sensitive to neuropeptides, were proposed to activate downstream from type-1 neurons. Hence this second phenotype was dubbed 'type-2' (Rekling et al., 1996b, a; Gray et al., 1999). We evaluated this classification scheme in *Dbx1*$^+$ and *Dbx1*$^-$ neurons in 9 mM K^+ ACSF and in low Ca^{2+} conditions.

We performed basic tests for delayed excitation indicative of I_A. Out of 48 *Dbx1*$^+$ neurons tested, 27 exhibited a 100-250 ms delay in the onset of spiking activity in response to a supra-threshold current step from a holding potential of approximately -80

mV (e.g., Fig. 2.6A). During this delay, the neurons exhibited a depolarizing ramp-like voltage trajectory, which suggests the slow inactivation of I_A (Hayes and Del Negro, 2007). After adjusting DC bias we injected the same net current during the 500-ms current step but observed no delay in the onset of spiking from a baseline of -50 mV. In

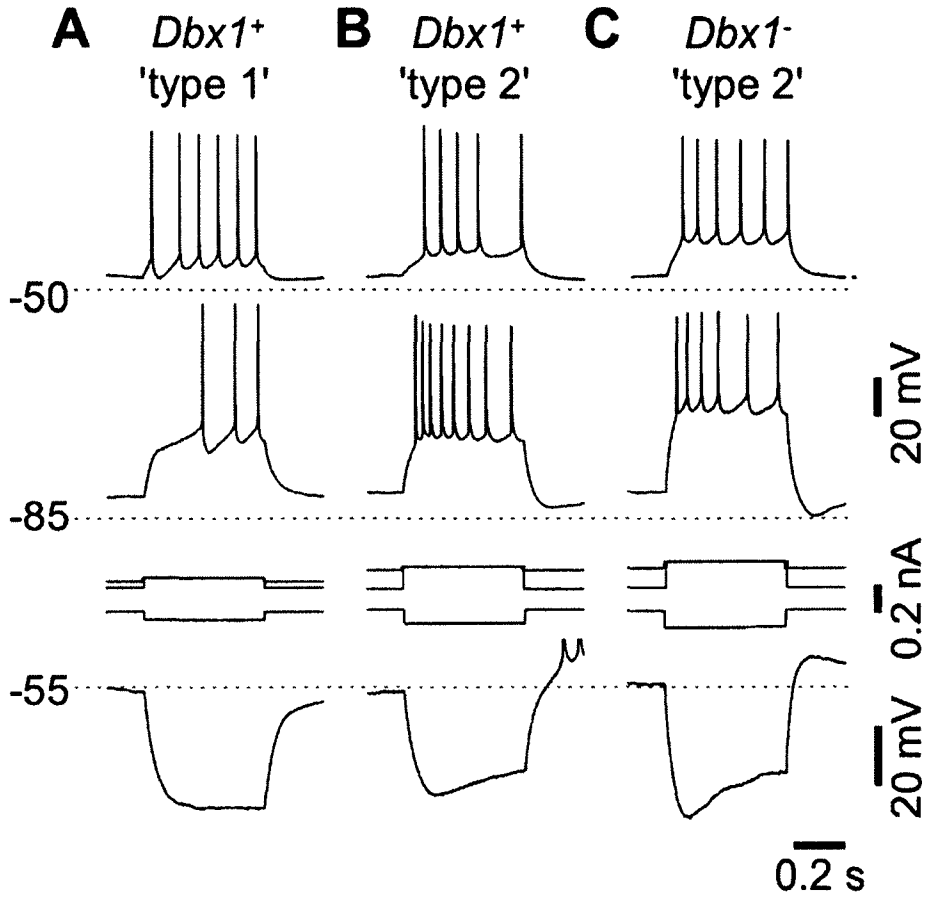

Figure 2.6 Delayed excitation and 'sag' potentials in *Dbx1*$^+$ (A and B) and *Dbx1*$^-$ (C) neurons. Depolarizing pulses (500 ms) were injected from a depolarized potential (above -50 mV) and from a hyperpolarized potential (near -85 mV). Hyperpolarizing pulses were injected from -55 mV. **A**, a type-1 *Dbx1*$^+$ neuron exhibiting delayed excitation from -85 mV, but not from -50 mV, and no sag potential in response to the hyperpolarizing pulse. **B** and **C**, a type-2 *Dbx1*$^+$ (B) and a *Dbx1*$^-$ (C) neuron exhibiting sag potentials but no delayed excitation. Spikes truncated above -50 mV in B (lowest trace).

contrast, 21 out of 48 *Dbx1*$^+$ (Fig. 2.6B) and 12 out of 16 *Dbx1*$^-$ (Fig. 2.6C) neurons showed no delay in the onset of spiking activity in response to 500-ms depolarizing current steps from a holding potential of -80 mV. The spike rate in these neurons (Fig. 2.6B,C) peaked at the onset of the current step and tended to accommodate thereafter

for the remainder of the current stimulus. Nor was there a delay in the onset of spiking in these *Dbx1*$^+$ and *Dbx1*$^-$ neurons in response to the same net current from a holding potential of -50 mV (Fig. 2.6B,C).

I_h causes a depolarizing 'sag' in the membrane potential trajectory, in response to a sustained hyperpolarizing step current. *Dbx1*$^+$ neurons that expressed I_A (20 out of 27) did not exhibit such a sag response (Fig. 2.6A). In contrast, there was a >10 mV sag response in 17 out of 21 *Dbx1*$^+$ (Fig. 2.6B) and 8 out of 12 *Dbx1*$^-$ neurons (Fig. 2.6C) that did not express I_A. Neurons showing sag potentials often exhibited post-inhibitory rebound at the end of the current pulse (Fig. 2.6B), which could be attributed to slow deactivation of I_h or possibly the de-inactivation of a low voltage-activated Ca^{2+} current (Elsen and Ramirez, 2005).

Table 2.2 Expression of delayed excitation and sag potential in *Dbx1*$^+$ neurons.

Dbx1$^+$ (n=48)	Sag	No Sag
Delayed Excitation	7 (15%)	20 (42%)
No Delayed Excitation	17 (35%)	4 (8%)

Table 2.3 Expression of delayed excitation and sag potential in *Dbx1*$^-$ neurons.

Dbx1$^-$ (n=16)	Sag	No Sag
Delayed Excitation	2 (12.5%)	2 (12.5%)
No Delayed Excitation	8 (50%)	4 (25%)

The expression of I_A and I_h showed a statistically significant tendency to be mutually exclusive in *Dbx1*$^+$ neurons, as suggested by the type-1 versus type-2

classification scheme (Rekling et al., 1996a, b; Gray et al., 1999). *Dbx1*$^+$ neurons exhibited delayed excitation without sag (type-1, Fig. 2.6A) or sag without delayed excitation (type-2, Fig. 2.6B) in comparable proportions (42%: 20 out of 48 tested, and 35%: 17 out of 48 tested, Table 2.2). Type-1 and type-2 *Dbx1*$^+$ phenotypes, as defined by mutually exclusive expression of I_A and I_h, occurred at significantly higher frequency than the two other possible 'types': delayed excitation and sag both present (15%: 7 out of 48 tested, Table 2.2) or delayed excitation and sag both absent (8%: 4 out of 48 tested, Table 2.2) (Fisher Exact test, $p < 0.001$). *Dbx1*$^-$ neurons (Fig. 2.6C) generally expressed the type-2 phenotype (50%: 8 out of 16 tested, Table 2.3). However, the other combinations including type-1 (12.5%: 2 out of 16 tested, Table 2.3), delayed excitation and sag both present (12.5%: 2 out of 16 tested, Table 2.3), and finally delayed excitation and sag both absent (25%: 4 out of 16 tested, Table 2.3) were observed at commensurate frequencies, so the relative prevalence of type-2 among *Dbx1*$^-$ neurons did not rise to statistical significance (Fisher Exact, $p > 0.05$).

Morphological properties

We imaged 23 *Dbx1*$^+$ and 14 *Dbx1*$^-$ biocytin-filled inspiratory neurons (Fig. 2.7A,B), and then performed 3D digital reconstruction in 14 *Dbx1*$^+$ and 12 *Dbx1*$^-$ neurons

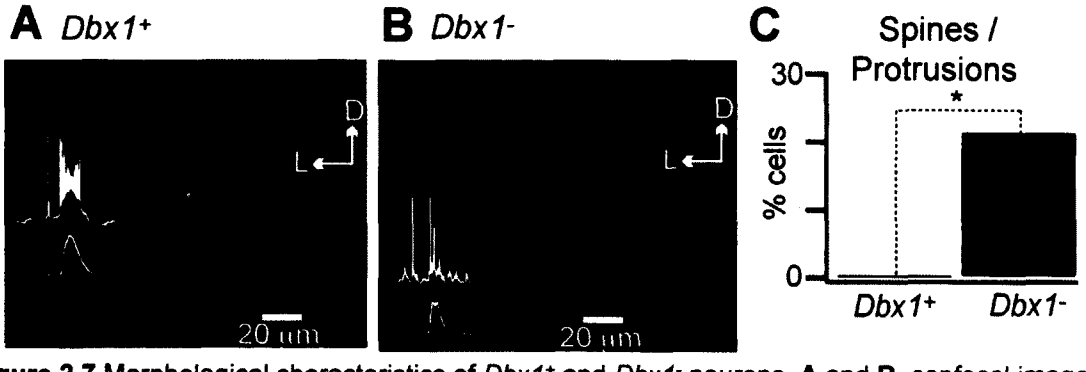

Figure 2.7 Morphological characteristics of *Dbx1*$^+$ and *Dbx1*$^-$ neurons. **A** and **B**, confocal images of biocytin-filled neurons processed with FITC-conjugated extravidin. *Dbx1*$^+$ (A) and *Dbx1*$^-$ (B) neuron in a *Dbx1*$^{+/CreERT2}$; *Rosa26*^{tdTomato} and a representative inspiratory burst and XII output (inset). **C**, Bar chart showing the percentage of *Dbx1*$^+$ and *Dbx1*$^-$ neurons with dendritic spines/ protrusions. Statistical significance indicated by * ($p < 0.05$).

(Figs. 2.8A-F and 2.9A-F). Out of the 39 morphological parameters measured, we selected a few principal measurements to report here. The *Dbx1*$^+$ and *Dbx1*$^-$ neurons were similar in surface area measurements. *Dbx1*$^+$ neurons measured 561 ± 48 μm^2 in soma surface area and 4769 ± 452 μm^2 in total somatodendritic surface area, whereas *Dbx1*$^-$ neurons measured 672 ± 59 μm^2 and 4008 ± 634 μm^2, respectively (t-test, $p > 0.05$ for both measurements). The dorsal-ventral span of dendrites measured on

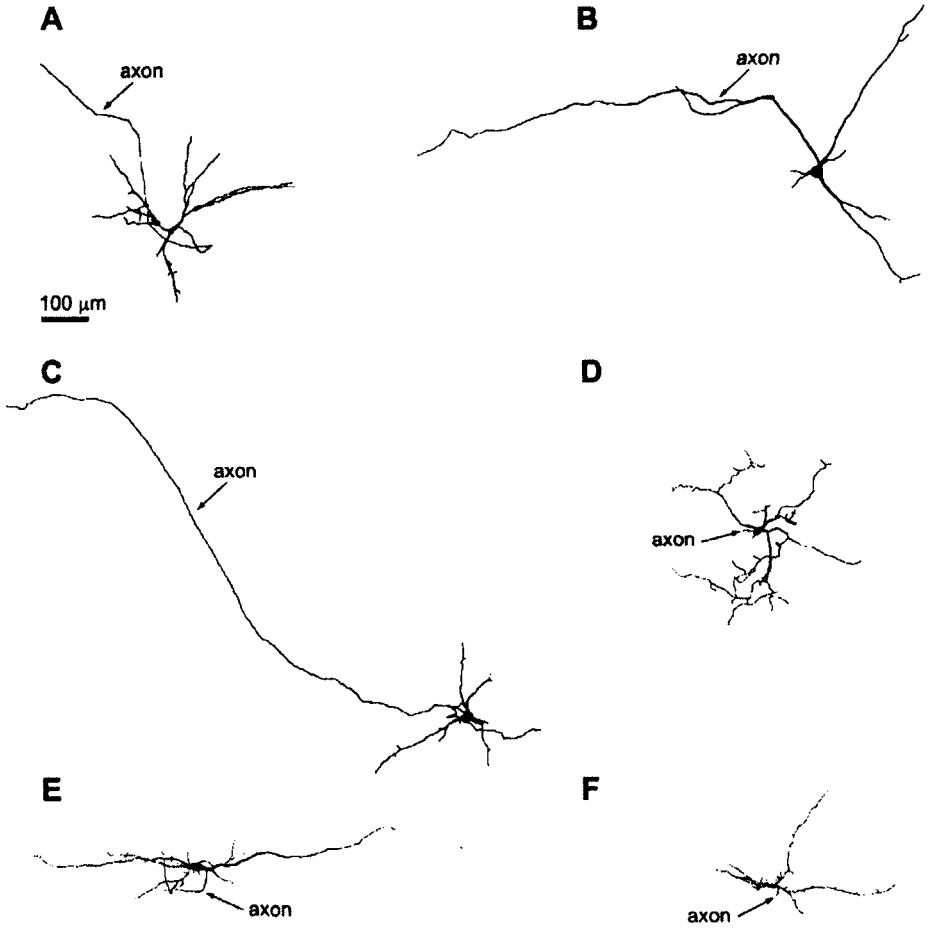

Figure 2.8 Digital reconstruction of *Dbx1*$^+$ (A-C) and *Dbx1*$^-$ (D-F) neurons in the transverse plane, with axons indicated. **A-C**, *Dbx1*$^+$ neurons obtained from the right preBötC, with axons that project leftward toward the midline consistent with bilateral connectivity. The axon of one *Dbx1*$^+$ neuron (C) crossed the midline of the slice. **D-F**, *Dbx1*$^-$ neurons obtained from the left preBötC, with axons that project short distances before truncation. F and Fig. 2.7B depict the same neuron. Scale bar applies to A-F.

average 269 ± 38 μm in *Dbx1*$^+$ neurons and 247 ± 21 μm in *Dbx1*$^-$ neurons, which was not significantly different (t-test, $p > 0.05$). The average medial-lateral span was also

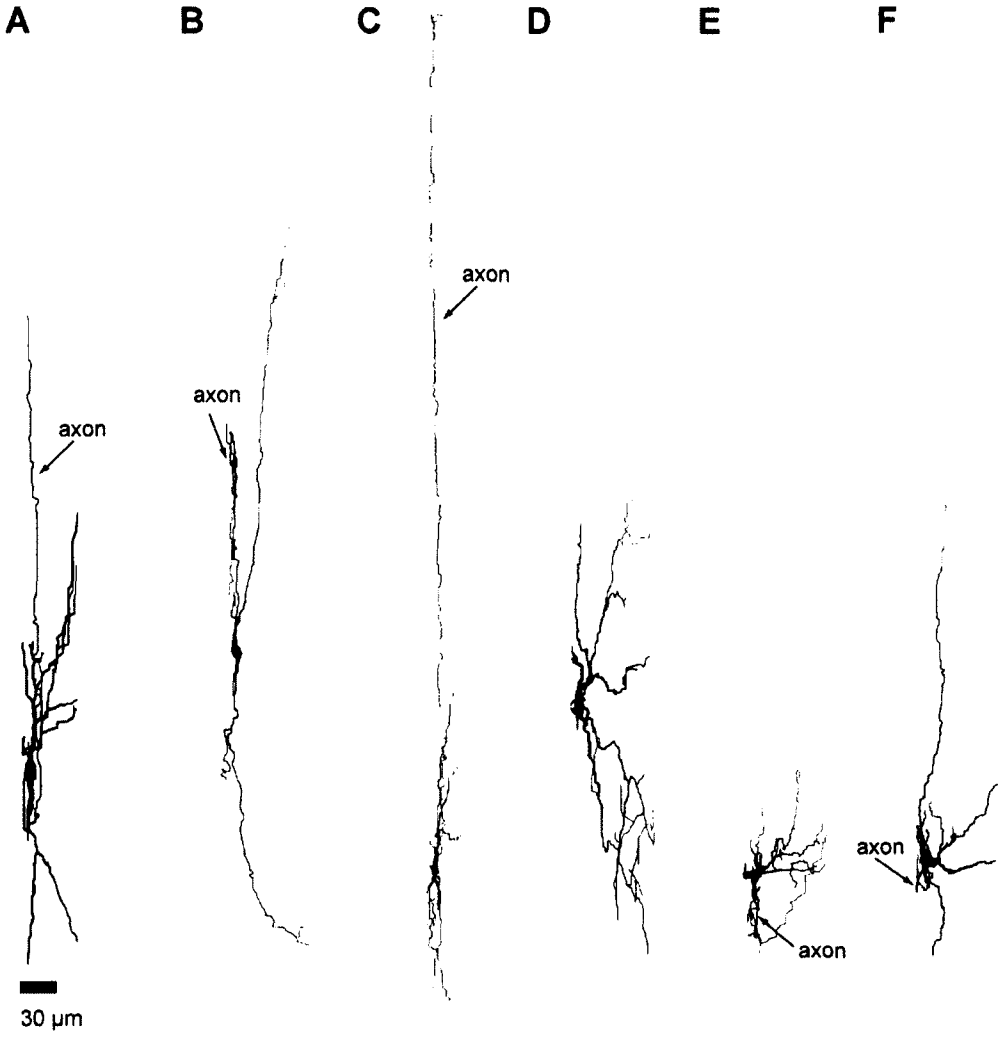

Figure 2.9 Digital reconstruction of *Dbx1*$^+$ and *Dbx1*$^-$ neurons in the parasagittal plane, with axons indicated. **A-C**, *Dbx1*$^+$ neuron. **D-F**, *Dbx1*$^-$ neurons. Scale bar applies to A-F.

comparable between the two groups (287 ± 38 µm in *Dbx1*$^+$ vs. 292 ± 43 µm in *Dbx1*$^-$, t-test, $p > 0.05$) (Fig. 2.8). Although *Dbx1*$^+$ and *Dbx1*$^-$ neurons did not appear to differ in size as measured in dorsal-ventral or medial-lateral orientations, the same was not true for projection in the parasagittal plane. The dendrites of the *Dbx1*$^-$ neurons extended deeper in the rostral-caudal axis, with a total average depth of 54 ± 4 µm, compared to an average total depth of 37 ± 4 µm for *Dbx1*$^+$ neurons (t-test, $p < 0.01$) (Fig. 2.9).

Dbx1$^-$ neurons appeared to have more branches (42 ± 8) compared to *Dbx1*$^+$ neurons (26 ± 4). The maximum branch order from the soma (soma is order 0; a branch that originates from the soma is order 1; second bifurcation from the same branch is order 2, and so on) was 8 ± 2 in *Dbx1*$^-$ neurons compared to 4 ± 0.4 in *Dbx1*$^+$ neurons. However, even though the number of branches and branch order differed by approximately two-fold, these differences were not statistically significant (t-tests, $p = 0.08$, Figs. 2.7 and 2.8).

The dendrites of *Dbx1*$^+$ neurons did not exhibit spines (Fig. 2.7A,C and 2.8A-C), whereas three out of 14 *Dbx1*$^-$ neurons (21%) showed spines and protrusions (Figs. 2.7B,C and 2.8D-F). This difference in the expression (or lack) of dendritic spines and protrusions was statistically significant (Fig. 2.7C, Fisher Exact, $p < 0.05$).

Eleven out of 23 *Dbx1*$^+$ neurons (48%) projected axons toward the midline, with one actually crossing the midline (Figs. 2.8A-C, 2.10). Two of the 14 (14%) *Dbx1*$^-$ neurons had axons projecting toward, yet none crossing, the midline (Fig. 2.8D-F, 2.10). In many cases, the axons of *Dbx1*$^-$ neurons appeared to be severed at the rostral face of the slice (which is identified by a bleb, significantly larger in diameter than its parent axon, at the immediate rostral surface of the slice preparation), suggesting a rostral projection path (n = 9 out of 14 *Dbx1*$^-$ neurons reconstructed). Nonetheless, the relative

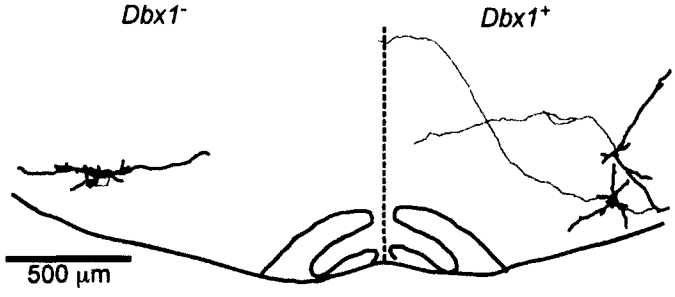

Figure 2.10 Morphology of *Dbx1*$^+$ (right) and *Dbx1*$^-$ (left) neurons obtained from the two preBötC sides of the same slice preparation. Two *Dbx1*$^+$ neurons from the right preBötC have their axons (red) cross/project towards midline, whereas the *Dbx1*$^-$ neuron has a truncated axon at the rostral face of the slice.

fraction of neurons with contralateral projections did not rise to statistical significance (Fisher Exact Test, $p > 0.05$).

2.4 DISCUSSION

Dbx1$^+$ neurons are an essential respiratory rhythmogenic population and the only source of non-catecholaminergic glutamatergic interneurons in the preBötC (Bouvier et al., 2010; Gray et al., 2010). Therefore, we may be able to elucidate the cellular mechanisms of rhythm generation through a comparative analysis of inspiratory *Dbx1*$^+$ and *Dbx1*$^-$ neurons in the preBötC. *Dbx1*$^+$ neurons differed from *Dbx1*$^-$ neurons mainly on the basis of properties measurable in the context of respiratory network activity, including larger inspiratory burst magnitude and earlier burst latency. The intrinsic membrane properties of *Dbx1*$^+$ neurons were notable for the tendency to express I_A and I_h in opposition, whereas *Dbx1*$^-$ neurons showed no consistent expression patterns of these intrinsic properties. Morphologically, *Dbx1*$^+$ neuron dendrites were smooth (spineless) and largely confined to the transverse plane, whereas *Dbx1*$^-$ neuron dendrites showed spines and protrusions, and spanned a greater distance in the parasagittal plane. We conclude that intrinsic conductances evoked in the context of ongoing network rhythmicity and dendritic properties may underlie the rhythmogenic nature of *Dbx1*$^+$ neurons.

Dbx1$^+$ neurons showed earlier inspiratory drive latency compared to *Dbx1*$^-$ neurons, and thus probably provide the 'on' switch of inspiration. This property is consistent with the pre-inspiratory activity reported for putative respiratory rhythmogenic neurons that were not identified by transmitter phenotype or gene expression patterns, but nonetheless showed drive latency of ~400 ms and were characterized by expression of I_A but lack of I_h, as well as neuropeptide sensitivity (Rekling et al., 1996a, b).

Furthermore, pre-inspiratory activity due to recurrent synaptic excitation has been proposed to be a key rhythmogenic feature based on intracellular studies *in vivo* and *in vitro* for 30 years (Richter, 1982; Ezure, 1990; Bianchi et al., 1995; Richter and Spyer, 2001; Feldman and Del Negro, 2006).

Dbx1$^+$ neurons also showed significantly larger magnitude drive potentials compared to *Dbx1*$^-$ neurons. The ionic mechanism underlying the larger inspiratory bursts can be gleaned from the observation that a significant number of *Dbx1*$^+$ neurons express intra-burst depolarization block. This type of behavior has been associated with the recruitment of I_{CAN}, which has been proposed to be important in inspiratory burst generation (Thoby-Brisson and Ramirez, 2001; Pena et al., 2004; Del Negro et al., 2005; Ramirez and Viemari, 2005; Rubin et al., 2009). We conclude that early drive latency and large burst magnitude are most likely attributable to recurrent excitation in the network and I_{CAN} expression in *Dbx1*$^+$ neurons, respectively. We suggest that these features are likely to be rhythmogenic because they are significantly different in *Dbx1*$^+$ compared to *Dbx1*$^-$ neurons of the preBötC.

PreBötC neurons that express I_A but lack I_h (dubbed type-1) were hypothesized to be primary rhythm generators based on their early drive latency (i.e., pre-inspiratory activity) and sensitivity to neuropeptide modulation. PreBötC neurons that express I_h but not I_A (dubbed type-2) were proposed to activate downstream from type-1 neurons (Rekling et al., 1996b, a; Gray et al., 1999; Hayes and Del Negro, 2007). In *Dbx1*$^+$ neurons we found that the expression of I_A and I_h showed a significant trend toward mutual exclusivity, consistent with Rekling et al.'s original classification scheme. *Dbx1*$^+$ neurons belong to either type-1 or type-2 in roughly equal numbers, and infrequently expressed I_A and I_h together or lacked expression of both. In contrast, *Dbx1*$^-$ neurons showed no consistent relationship regarding I_A and I_h expression (although the type-2

phenotype: lack of I_A in conjunction with expression of I_h was the most frequently observed at 50%).

Since a significant fraction of *Dbx1*$^+$ neurons shows a type-1-like complement of intrinsic properties and type-1 neurons have been hypothesized to be rhythm generators, then why might the *Dbx1*$^+$ type-1 phenotype be rhythmogenic? The combination of I_A and I_h in *Dbx1*$^+$ neurons could be important for rhythmogenesis if these expression patterns apply to dendrites. Hayes and Del Negro (2007) previously measured somatic I_A in outside-out patches and whole-cell recordings, and proposed that this intrinsic current prevents recurrent excitatory input from causing the membrane potential to cross spike threshold prematurely during the pre-inspiratory phase. If expressed dendritically in *Dbx1*$^+$ neurons, I_A could play a complementary role to activate at or above threshold and prevent spurious dendritic plateau-like depolarizations that cause somatic bursts, as previously shown in CA1 pyramidal neurons (Hoffman et al., 1997; Acker and White, 2007). We propose that I_A acts to suppress premature bursts and thus promotes an orderly ramp-like trajectory during the pre-inspiratory phase. I_h in CA1 neuron dendrites, by contrast, limits subthreshold temporal summation, allowing proximal and distal inputs to produce the same temporal output patterns (Magee, 1999; Migliore et al., 2004). Therefore, it may be desirable to preclude I_h expression in *Dbx1*$^+$ interneurons of the preBötC to promote temporal summation of subthreshold inputs in dendrites. We propose that the presence of I_A and lack of I_h could be important properties of the type-1 population that may prevent spurious burst discharge and yet promote temporal summation in type-1 *Dbx1*$^+$ neurons during the pre-inspiratory interval, but this hypothesis remains to be fully tested by direct recordings in dendrites and via computer simulation.

Type-2 neurons were proposed to activate downstream from type-1 neurons, and in that regard may play a premotor role in respiratory network activity. Because *Dbx1*$^{+}$ neurons are found in a continuous line from the dorsomedial to ventrolateral region of the transverse section (Bouvier et al., 2010; Gray et al., 2010), many *Dbx1*$^{+}$ neurons lie within the intermediate region between the preBötC and the XII nucleus, which is known to contain respiratory premotor neurons (Koizumi et al., 2008; Volgin et al., 2008). Type-2 *Dbx1*$^{+}$ neurons may participate in a paucisynaptic pathway from type-1 rhythmogenic neurons to XII motoneurons, which may involve premotor neurons in the intermediate regions of the medulla between preBötC and the XII nucleus, but this too remains to be demonstrated. Nevertheless, given that *Dbx1*$^{+}$ neurons in *Dbx1*^{CreERT2};*tdTomato* mice can be visualized in the dorsal-ventral region between the preBötC and the XII motor nucleus, it would be possible to obtain recordings from *Dbx1*$^{+}$ neurons intercalated in this region where premotor respiratory neurons have been found in wild-type rats (Koizumi et al., 2008).

One-fifth (i.e., 20%) of all neurons in the preBötC including *Dbx1*$^{+}$ glutamatergic neurons (this paper), glycinergic neurons (Morgado-Valle et al., 2010), and NK1R-expressing neurons (Pagliardini et al., 2005) – which constitute overlapping subpopulations – express voltage-dependent bursting properties. Although I_{NaP} expression in the preBötC is higher than adjacent regions of the medulla (Ptak et al., 2005), the voltage-dependent bursting engendered by I_{NaP} / $I_{K\text{-}Leak}$ ratio does not differentiate the critical *Dbx1*$^{+}$ population from the *Dbx1*$^{-}$ population and thus we conclude that voltage-dependent bursting properties are less likely to constitute a key rhythmogenic feature of *Dbx1*$^{+}$ neurons.

Dbx1^{+} neurons are identical in basic membrane properties (tau_M, R_N, and C_M) to *Dbx1*$^{-}$ neurons, but have lower rheobase$_{-60}$ in the context of network activity. *Dbx1*$^{+}$

neurons may be 'primed' by ongoing synaptic activity acting via metabotropic receptors and intracellular signaling, which would enhance excitability and facilitate spike discharge, resulting in a lower threshold and rheobase. However, in type-1-like *Dbx1*$^+$ neurons the lower rheobase may be mitigated by expression of I_A. If the role of I_A is to appropriately delay the onset of plateau-like depolarization in support of inspiratory burst generation, then a lower rheobase may be important to ensure robust spiking at the onset and during inspiratory bursts.

We identified commissural projections of *Dbx1*$^+$ neurons, which is consistent with the previous finding that *Dbx1*$^+$ interneurons bilaterally synchronize the preBötC (Bouvier et al., 2010). Some *Dbx1*$^-$ neurons showed contralateral projections, but most did not. In many instances, the lack of contralateral projections reflects axotomy due to transverse slicing. This suggests that the *Dbx1*$^-$ population projects rostrocaudally, rather than locally in the bilaterally distributed preBötC, and thus may be involved in modulating rostral respiratory nuclei, including the Bötzinger complex (BötC, an expiratory relay center) of the VRC and the RTN/pFRG (defined in Chapter 3), among others. In that regard, the inspiratory bursts of *Dbx1*$^-$ neurons may provide a mimic of preBötC activity to influence or possibly inhibit other sites and nuclei via rostrally projecting axons.

Dbx1$^+$ neurons have dendrites largely confined to the transverse plane, which may facilitate local synaptic integration among the bilaterally projecting *Dbx1*$^+$ subpopulation. This is consistent with *Dbx1*$^+$ neurons underlying the network of interconnected propriomedullary interneurons in the preBötC (Ellenberger and Feldman, 1990; Dobbins and Feldman, 1994). The *Dbx1*$^-$ neurons extend their dendritic arbor outside the plane of section, deeper in the rostral-caudal axis. Although speculative, this may be related to connectivity with rostral and/or caudal structures.

Dbx1$^+$ neurons have fewer branches with no spines, whereas *Dbx1*$^-$ neurons show spines and protrusions. While this observation needs further evaluation, smooth unbranched dendrites may promote signal conduction in the dendrites, which would help retain the amplitude of synaptic input as it propagates from dendrite to soma (Rall and Agon-Snir, 1998). This correlates with the observation that *Dbx1*$^+$ have larger magnitude drive potentials than *Dbx1*$^-$ neurons. Spines and protrusions have been previously reported on inspiratory preBötC neurons (Koizumi et al., 2008). Our results suggest that the spiny neurons are not *Dbx1*-derived and likely not glutamatergic, and thus could possibly be inhibitory preBötC neurons.

We previously showed that some *Dbx1*$^-$ neurons within the preBötC are Lmx1b-derived catecholaminergic neurons (of the C1 group) essential in modulating blood pressure and cardiovascular function, but unlikely implicated in respiratory rhythm generation (Gray et al., 2010). Since half of the inspiratory neurons in the preBötC are inhibitory glycinergic neurons (Winter et al., 2009), the *Dbx1*$^-$ neurons that we recorded are most likely glycinergic neurons presumably derived from *Lbx1*, the TF shown to be essential for development of glycinergic neurons in the ventral medulla (Pagliardini et al., 2008). We also acknowledge the possibility of incomplete Cre recombination and that some of the recorded *Dbx1*$^-$ neurons were actually *Dbx1*-derived neurons that were not labeled by the reporter protein. We induced Cre recombination by administering tamoxifen at E10.5 to obtain robust reporter expression of *Dbx1* neurons in the hindbrain (Hirata et al., 2009; Gray et al., 2010). However, since *Dbx1* is expressed at E9.5 in the mouse brain and spinal cord (Lu et al., 1992; Shoji et al., 1996), and even observed as early as E8.5 in small subsets of the forebrain (Causeret et al., 2011), then the *Dbx1*$^+$ cells that appear earlier than the tamoxifen induction of Cre would not be labeled by the fluorescent protein. These non-fluorescent neurons, that are actually *Dbx1*-derived, could constitute a subset of recorded *Dbx1*$^-$ neurons that exhibited rhythmic properties

equally or even more robust than the average *Dbx1*$^{+}$ neuron. However, given the distinct differences in their morphology, we think it is unlikely that our *Dbx1*$^{-}$ subpopulation is dominated by false negative *Dbx1*$^{+}$ unlabeled by the reporter, and is more likely representative of the glycinergic subpopulation (Winter et al., 2009; Morgado-Valle et al., 2010).

In summary, we evaluated the membrane properties of genetically-identified rhythm-generating neurons in the preBötC of transgenic mice to help unravel the cellular mechanisms of respiratory rhythmogenesis. We propose that the rhythmogenic properties of *Dbx1*$^{+}$ neurons originates from a higher level of intrinsic excitability that allows temporal summation of incoming excitatory synaptic inputs necessary for generating robust inspiratory bursts. Furthermore, *Dbx1*$^{+}$ neurons exhibit a functional morphology that may facilitate integration of local synaptic inputs from other *Dbx1*$^{+}$ neurons, which could be important for initiating and maintaining bursts and synchronizing activity during the inspiratory phase.

CHAPTER 3. Role of *Math1*-derived neurons in coordinating respiratory activity

3.1 INTRODUCTION

The Mouse Atonal Homolog 1 (*Math1, Atoh1*) is one of the transcription factors that has been demonstrated to play an important role in the development of respiratory network function. Along with *Dbx1* (see Chapter 2), *Math1* is expressed in the RTN/ pFRG, which comprises a mixed population of neurons from the retrotrapezoid nucleus (RTN) (Smith et al., 1989), which is important in chemoreception (Smith et al., 1989; Stornetta et al., 2006; Guyenet et al., 2009), and neurons of the parafacial respiratory group (pRFG), which is the putative site of active expiration (Mellen et al., 2003; Onimaru and Homma, 2003; Janczewski and Feldman, 2006; Pagliardini et al., 2011). In mice, *Math1* is expressed in the progenitor domain DA1 (see Chapter 1, Fig. 1.1) in the dorsalmost portion of the neural tube. Furthermore, *Math1* is required in postmitotic DB2 neurons for proper migration and development of RTN/pFRG neurons, including those that express the TF dubbed paired-like homeobox 2b (*Phox2b*) (Rose et al., 2009a; Rose et al., 2009b; Ramanantsoa et al., 2011). Phox2b-expressing (*Phox2b*$^{+}$) neurons in the RTN/pFRG, that also co-express neurokinin1 receptors (NK1R), play an important role in central chemoreception (Nattie and Li, 2006; Dubreuil et al., 2008; Takakura et al., 2008), and may play a role in rhythm generation, although the exact nature of the rhythm - expiratory versus inspiratory - is incompletely understood from the standpoint of perinatal developmental (Onimaru et al., 2008; Thoby-Brisson et al., 2009; Onimaru et al., 2012).

Loss of *Math1* disrupts multiple components of the auditory, proprioceptive, interoceptive, and arousal systems as well as several respiratory-modulating neurons in the hindbrain (Ben-Arie et al., 1997; Machold and Fishell, 2005; Wang et al., 2005; Rose et al., 2009b). Mutant mice lacking the *Math1* gene appear to have normal lungs,

airways and peripheral nerves, yet they die shortly after birth due to compromised glutamatergic excitatory drive, which prevents the initiation of normal respiration (Rose et al., 2009b). *Math1*-derived (*Math1*$^+$) neurons also project to the area of the preBötC. However, the lack of *Math1* does not seem to affect the rhythmogenic *Dbx1*$^+$ neurons or the excitatory glutamatergic transmission within the preBötC (Rose et al., 2009b). This suggests that *Math1* is important but not necessary for generating the inspiratory rhythm *in vitro*. Nevertheless, *Math1* mutant mice cannot sustain respiration so the nature and mechanism of *Math1*$^+$ neuron contributions to normal breathing is a key problem in respiratory neurobiology.

The respiratory network is proposed to consist of two coupled oscillators: a dominant inspiratory CPG in preBötC (Smith et al., 1991; Feldman and Del Negro, 2006) and an expiratory network that can be active or quiescent as physiological conditions demand (Mellen et al., 2003; Onimaru and Homma, 2003; Janczewski and Feldman, 2006; Abbott et al., 2011; Pagliardini et al., 2011). *In vitro* preparations of the brainstem and spinal cord generate inspiratory-related (I) motor nerve output from the cervical roots (C3-C5) that make up the phrenic nerve innervating the diaphragm, and expiratory (E) output from the first lumbar root (L1) that innervates the abdominal muscles that compress the abdomen for forced expiratory efforts. Both C3-C5 and L1 outputs are strongly coupled with a consistent phase lag. Unlike *Dbx1*$^+$ neurons, which are important for both inspiratory and expiratory behaviors (Gray et al., 2010), *Math1*$^+$ neurons are not necessary for either I or E output *in vitro,* but could play a role in coordinating the rhythm and pattern of respiratory activity (Tupal et al., 2012), in particular *Math1*$^+$ neurons could influence normal cervical-lumbar (I/E) temporal delay.

In this Chapter, we look at the potential role of *Math1*$^+$ neurons in influencing the pattern of the respiratory rhythm. We propose that the relative phase of the I and E

oscillators is modulated by glutamatergic *Math1*$^{+}$ excitatory neurons intercalated between the inspiratory rhythmogenic preBötC and the rhythmogenic (putatively expiratory) center of the RTN/pFRG. To test this hypothesis, we record from slices that exclude the RTN/pFRG yet capture the *Math1*$^{+}$ population rostral to the preBötC. This allows us to analyze the relationship of the *Math1*$^{+}$ neurons to preBötC activity, and glean functional network connectivity as a first level analysis of the specific role of *Math1*$^{+}$ neurons in respiration. In addition, we analyze the morphology of *Math1*-derived neurons to explore whether they exhibit cellular properties consistent with a function in coordinating respiratory activity.

3.2 MATERIALS AND METHODS

The following protocols have been approved by the Institutional Animal Care and Use Committee at The College of William & Mary. We used transgenic mice that express the cre recombinase *Math1*^{Cre} and floxed *Rosa26*^{EYFP} reporter mice that express enhanced yellow fluorescent protein (EYFP). Positive neonates were identified by the fluorescent signal from the cerebellum and hindbrain.

We anesthetized and then dissected neonatal *Math1*^{Cre}; *Rosa26*^{EYFP} at postnatal day 0 to 2 (P0-2) in standard artificial cerebrospinal fluid (ACSF) containing (in mM): 124 NaCl, 3 KCl, 1.5 $CaCl_2$, 1 $MgSO_4$, 25 $NaHCO_3$, 0.5 NaH_2PO_4, and 30 dextrose, equilibrated with 95% O_2 and 5% CO_2 (pH 7.4). Transverse 550-µm-thick brainstem slices were cut to place the rostral ventral respiratory column (rostral to the preBötC yet excludes the RTN/pFRG) at the slice surface using a vibrating microtome. Slices were perfused with ACSF at 26-28 °C in a recording chamber on a fixed-stage Zeiss Axioskop with infrared-enhanced differential interference contrast (IR-DIC) imaging and

epifluorescence, which enables visual identification and selective recording of target neurons.

Electrophysiology

Rhythmic respiratory-related motor output was recorded from the XII nerve rootlets, which were captured with the preBötC in transverse slices, using suction electrodes and a differential amplifier. Amplifier gain was set at 2000 and the bandpass filter was set at 300-1000 Hz (Dagan Instruments). The XII discharge was full-wave rectified and smoothed for display. On-cell and whole-cell patch-clamp recordings were obtained using patch pipettes with resistance of 4-6 MΩ and a Dagan IX2-700 current-clamp amplifier. IR-DIC imaging was used to target patch pipettes after fluorescent identification of *Dbx1*$^{+}$ neurons. All recordings were digitally acquired at 10 kHz using a PowerLab 16-bit A/D converter after 1 kHz low-pass filtering (AD Instruments.

The patch solution contained (in mM): 140 K-Gluconate, 10 HEPES, 5 NaCl, 1 $MgCl_2$, 0.1 EGTA, 2 Mg-ATP and 0.3 Na(3)-GTP and 2 mg/ml biocytin (B4261, Sigma Aldrich). We added 50 µM of Alexa 568 (A10436, Invitrogen) hydrazide dye to the patch solution for fluorescent visualization of *Rosa26*^{EYFP}-labeled neurons recorded in the whole-cell configuration.

The membrane time constant (tau_M) was fitted by regression to an exponential decay function based on the membrane voltage response to a 500 ms hyperpolarizing current pulse from a baseline membrane potential of -60 mV. To obtain input resistance (R_N), we applied 1 s current steps from -60 mV in a 10-step sequence. We plotted the resulting voltage-current relationship (VI) and measured its slope in the linear region between (approximately) -95 and -55 mV. The whole-cell capacitance (C_M) was calculated using R_N and tau_M.

Morphological reconstruction

Slices containing biocytin-loaded neurons were fixed in 4% paraformaldehyde in 0.1 M Na-phosphate buffer for at least 16 hours at 4°C. Slices were washed 3 times for 15 minutes each in PBS + 1% Triton X-100 and then blocked in 10% heat-inactivated fetal bovine sera (F4135, Sigma Aldrich) for 45 minutes. Finally, the slices were incubated in FITC-conjugated extravidin (E2761, Sigma Aldrich) for 2-4 hours, rinsed with PBS and coverslipped in Vectashield (H-1500, Vector Laboratories). We visualized recorded neurons using a laser-scanning confocal microscope (Zeiss LSM 510). Images were contrast enhanced and pseudocolored using the free ImageJ software (National Institutes of Health), and then digitally reconstructed using the freeware Neuromantic reconstruction tool (Myatt et al., 2012). The 3-D digital reconstructions functioned as tree-like digital objects that we further analyzed according to 39 different measurements using the freeware L-measure (Scorcioni et al., 2008).

3.3 RESULTS

Whole Cell Recordings

We studied the cellular properties of *Math1*$^{+}$ neurons using brainstem slice preparations from *Math1*^{Cre};*Rosa26*^{EYFP} neonatal mice (n = 3), postnatal ages 0-2 (P0-

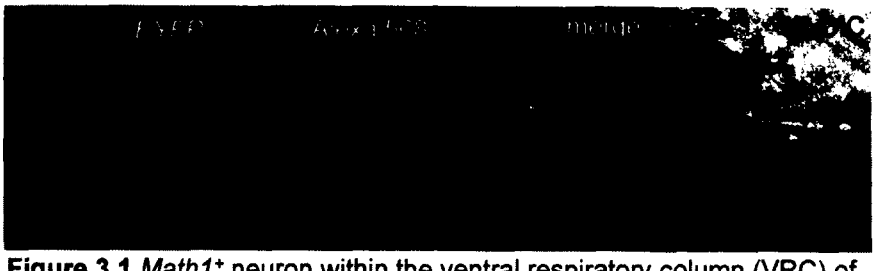

Figure 3.1 *Math1*$^{+}$ neuron within the ventral respiratory column (VRC) of *Math1*$^{+/Cre}$; *Rosa26*^{EYFP} brainstem slice preparation. **L-R**, EYFP-labeled *Math1*$^{+}$ neuron, Alexa 568-filled, merged fluorescence, and IR-DIC images.

P2). We performed whole-cell patch-clamp intracellular recordings from visually identified *Math1*$^+$ neurons (n = 6). In all cases, we verified recording of intended EYFP-labeled *Math1*$^+$ neuron by filling it with Alexa 568 and merging two images (EYFP and Alexa 568) to make a composite figure that demonstrates co-localization (Fig. 3.1).

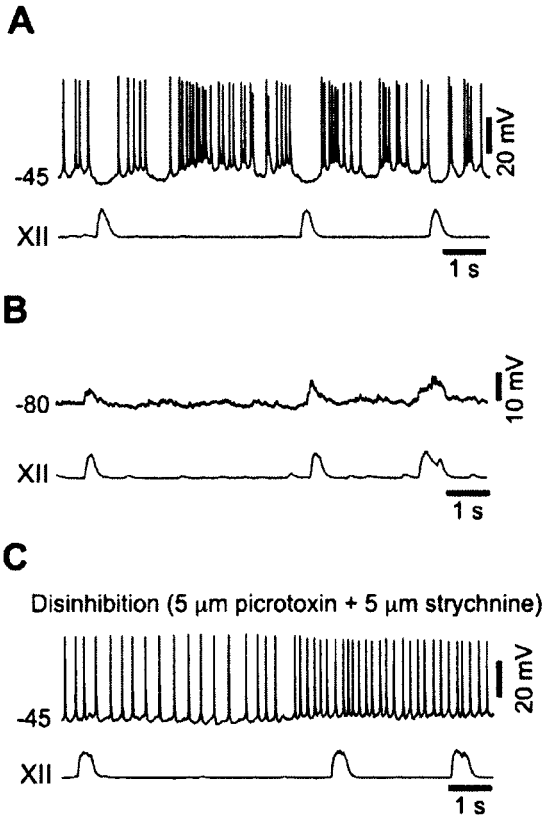

Figure 3.2 Whole-cell recording (upper) and XII output (lower) of respiratory modulated *Math1*$^+$ neuron. **A**, Expiratory activity at baseline membrane potential of -45 mV. **B**, Depolarizations at hyperpolarized membrane potential of -80 mV. **C**, Tonic spiking after disinhibition with 5 μm picrotoxin and 5 μm strychnine.

One of the six *Math1*$^+$ neurons showed expiratory activity at its -45 mV baseline membrane potential (Fig. 3.2A, upper traces). The neuron exhibited tonic spiking activity and burst-like discharge during the inter-inspiratory burst intervals (i.e., between cycles of XII output), punctuated by transient hyperpolarizations in sync with the XII motor output. At hyperpolarized voltages (baseline at -80 mV), the neuron showed 5-10 mV depolarizations, which are consistent with reversed IPSPs since the chloride reversal

potential is approximately -70 mV under our recording conditions (Fig. 3.2B). After addition of 5 μm picrotoxin and 5 μm strychnine to the bath-perfusion solution, the same *Math1*$^+$ neuron exhibited tonic spiking without any apparent respiratory modulation (Fig. 3.2C), which is again consistent with active chloride-mediated inhibition of *Math1*$^+$ neurons during the inspiratory phase of the respiratory cycle.

The results presented here are preliminary and from a small data set therefore, for the purpose of analyses, we compared the measurements in the single respiratory modulated neuron with the average measurements from the non-respiratory modulated neurons. We recorded intrinsic membrane properties, which include the time constant (tau_M), input resistance (R_N) and whole cell capacitance (C_M) of the *Math1*$^+$ neurons. There were not enough reliable measurements to quantify rheobase. No considerable difference in membrane properties was observed between the respiratory modulated and non-respiratory modulated *Math1*$^+$ neurons. For the tau_M, the respiratory neuron measured 44 ms, while the non-respiratory modulated average was 33 ± 4 ms (group mean [including the expiratory *Math1*$^+$ neurons] measured 35 ± 4 ms). The respiratory modulated neuron had a R_N of 353 MΩ which was comparable to the non-respiratory modulated average of 392 ± 80 MΩ (group mean = 384 ± 62 MΩ). Lastly, C_M measured 124 pF in the respiratory modulated neuron and 89 ± 10 pF for the non-respiratory modulated neurons (group mean = 96 ± 11 pF).

Morphology

We analyzed the morphology of *Math1*$^+$ neurons to look for clues with regard to their potential role in coordinating activity in the respiratory network. We compared the morphology of the respiratory modulated *Math1*$^+$ neuron with the non-respiratory modulated neurons to determine whether there could be any differences in their features

that might contribute to our knowledge in elucidating the function of *Math1*$^+$ neurons in phasing inspiration and expiration.

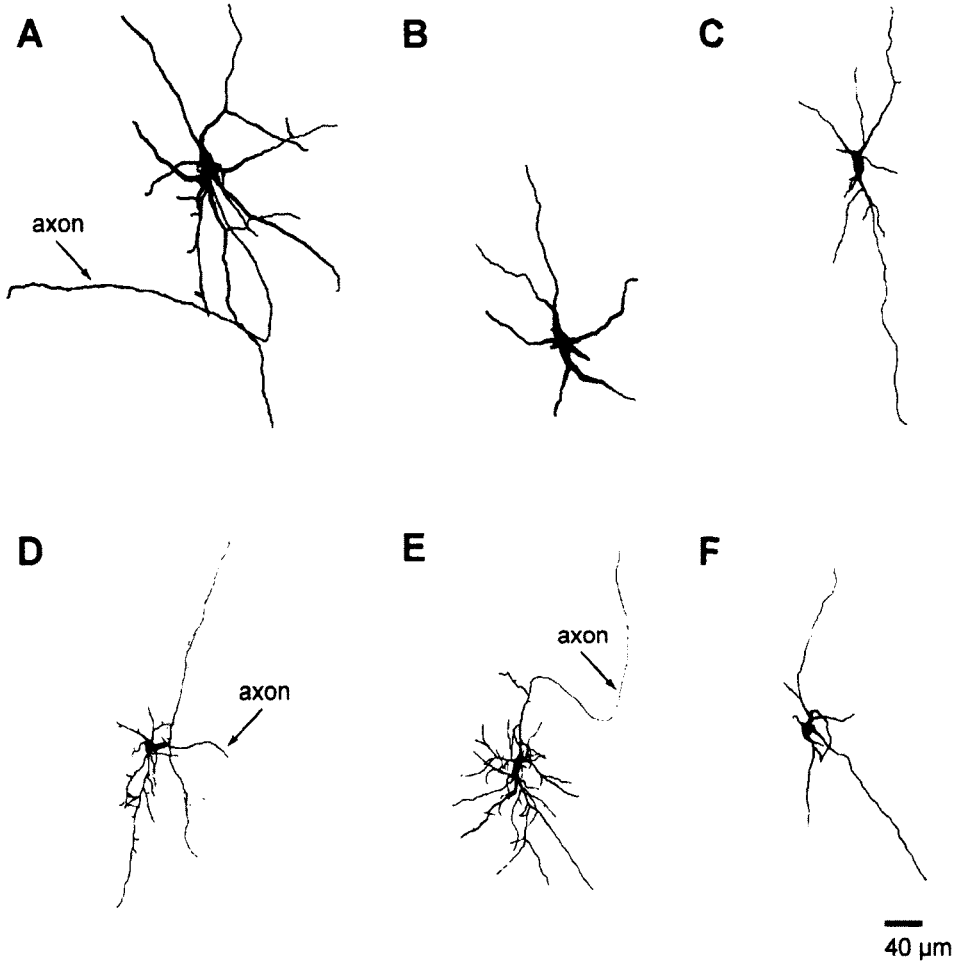

Figure 3.3 Digital reconstruction of the *Math1*$^+$ neurons in the transverse plane, with axons indicated. **A**, Respiratory modulated *Math1*$^+$ neuron. **B-F**, Non-respiratory modulated *Math1*$^+$ neurons. Scale bar applies to A-F.

We imaged and digitally reconstructed one respiratory modulated and five non-respiratory modulated *Math1*$^+$ neurons. Figure 3.3 shows the morphology of the six *Math1*$^+$ neurons in the transverse plane. Overall, the respiratory modulated *Math1*$^+$ neuron (Fig. 3.3A) had a larger surface area compared to the non-respiratory modulated *Math1*$^+$ neurons (Fig. 3.3B-F). The soma surface area of the respiratory modulated neuron was larger compared to the average soma size of the non-respiratory modulated neurons (5024 µm^2 versus 908.6 µm^2). Moreover, the total somatodendritic surface area

measured 27137 μm^2 for the respiratory modulated neuron and only 6915 μm^2 in the average non-respiratory modulated neurons.

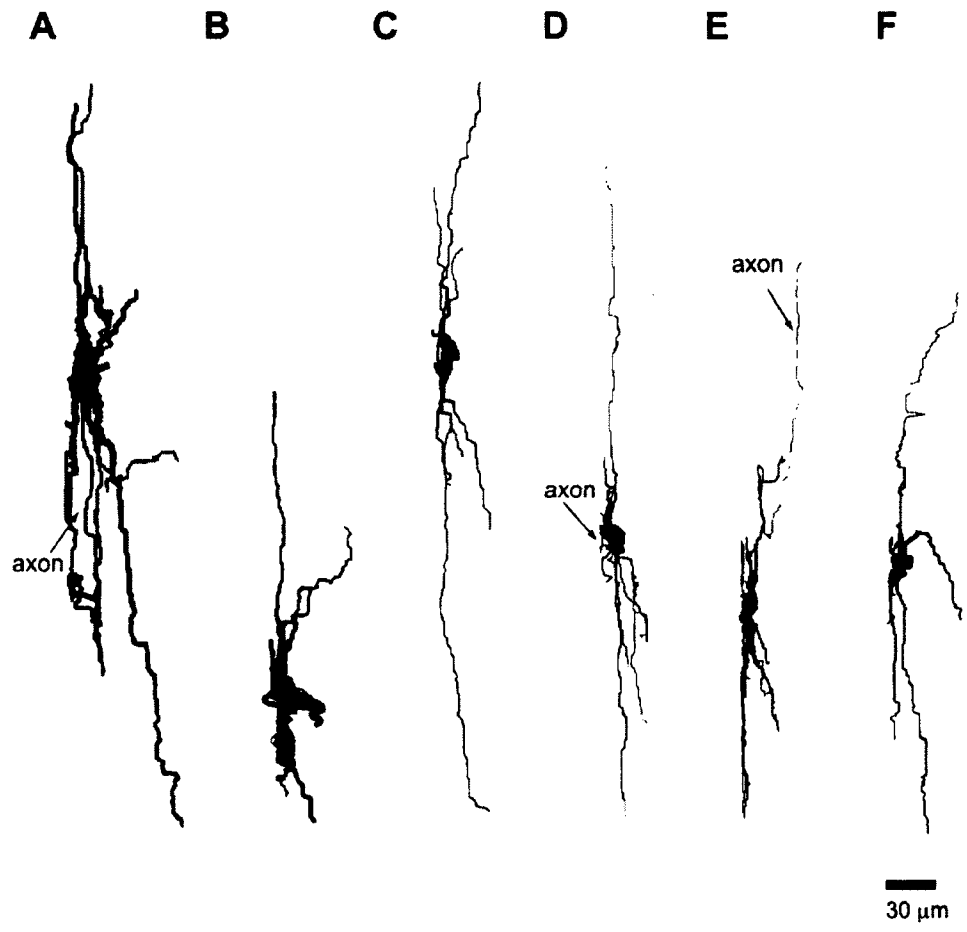

Figure 3.4 Digital reconstruction of *Math1*$^+$ neurons in the parasagittal plane, with axons indicated. **A**, Respiratory modulated *Math1*$^+$ neuron. **B-F**, Non-respiratory modulated *Math1*$^+$ neurons. Scale bar applies to A-F.

We supplemented the total surface area measurements by specifically measuring the medial-lateral span (width, x), dorsal-ventral span (height, y) and rostral-caudal span (depth, z) of the six *Math1*$^+$ neurons. The respiratory modulated neuron had a larger height of 417 µm whereas the average height of the non-respiratory modulated neurons was 339 µm. The width of the respiratory-modulated neuron was 333.6 µm, whereas width measured less than half (141.8 µm) for the average non-respiratory modulated neurons. In addition, the respiratory modulated neuron extended deeper in the z-axis

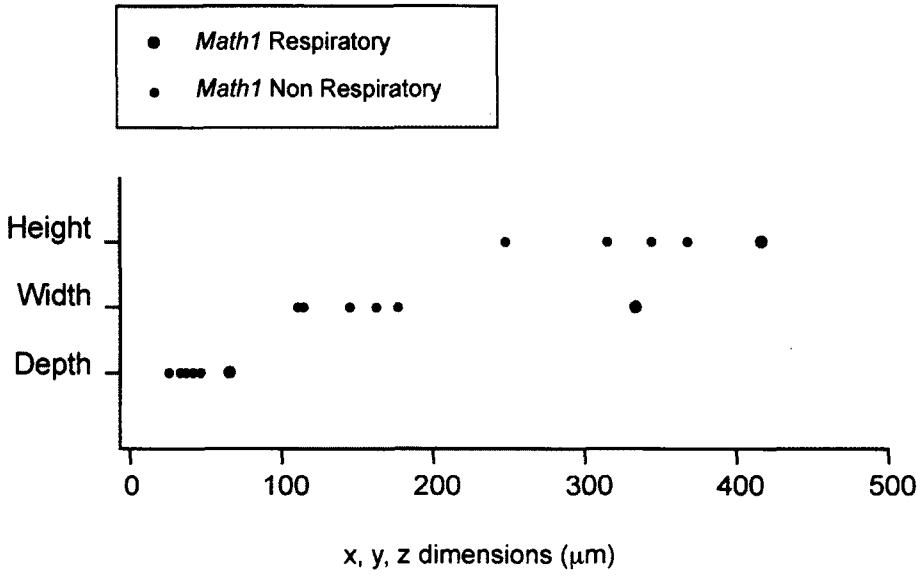

Figure 3.5 Morphology of the *Math1*$^+$ neurons. Plot chart showing the height (dorsal-ventral, y-axis), width (medial-lateral, x-axis) and depth (rostral-caudal, z-axis) of the respiratory (red dots) and non-respiratory modulated (black dots) *Math1*$^+$ neurons.

(parasagittal plane) than the average non-respiratory modulated neuron (65.6 μm versus 36.9 μm, Fig. 3.4). Furthermore, the total straight line (Euclidean) distance from the soma to the tip of the longest branch was 104 μm in the respiratory modulated neuron and only 79 μm in the average non-respiratory modulated neuron.

Figure 3.5 plots the height, width and depth measurements of the six *Math1*$^+$ neurons. The data show that the respiratory modulated *Math1*$^+$ neuron measures considerably larger in the x, y and z axes compared to the non-respiratory modulated neurons. On the other hand, the respiratory modulated *Math1*$^+$ neuron appears to exhibit slightly less branching and fewer bifurcations. Compared to the average non-respiratory modulated neuron with 45 branches and 20 bifurcations, the respiratory modulated neuron had only 32 branches and 14 bifurcations. More samples are needed to determine whether the difference in measurements between respiratory and non-respiratory modulated *Math1*$^+$ neurons are statistically significant. Nevertheless, the overall mass of the respiratory modulated *Math1*$^+$ neuron suggests that respiratory and

non-respiratory modulated *Math1*$^+$ neurons may be differentiable on the basis of morphology.

3.4 DISCUSSION

We examined the potential role of *Math1*$^+$ neurons in shaping the pattern of respiratory rhythm by studying their electrophysiological and morphological properties. Although our results are preliminary, the information obtained in the study may provide an initial cellular characterization of *Math1*$^+$ neurons and thus represents a first step in elucidating their role in the generation and coordination of respiratory rhythm.

In vitro brainstem and spinal cord preparations generate inspiratory output from the cervical roots and expiratory output from the lumbar roots, with a consistent temporal delay, where the expiratory output precedes inspiratory output. *Math1* mutant mice cannot temporally separate the lumbar and cervical outputs, suggesting that the time lag could be influenced by the *Math1*$^+$ population (Tupal et al., 2011; Tupal et al., 2012). We characterized the *Math1*$^+$ population in the VRC to uncover any property that might elucidate this temporal coordination between the inspiratory and expiratory outputs.

One out of six *Math1*$^+$ neurons we recorded exhibited respiratory modulation. The respiratory modulated *Math1*$^+$ neuron (n = 1) was located in the VRC just rostral to the preBötC yet caudal to the pFRG, and could belong to a group of recently discovered early-forming *Math1*$^+$ neurons that develop at E10.5 and also express the TF *Lhx9* (Rose et al., 2009a). The rhythmic *Math1*$^+$ neuron exhibited expiratory tonic spiking activity with phasic inhibition during inspiration, thus we propose that there exists a projection from the preBötC that inhibits the rhythmic *Math1*$^+$ neuron. Similar to the rhythmic *Math1*$^+$ neuron that we recorded, some cells in the pFRG region that exhibit late-expiratory (late-E) and post-inspiratory (post-I) activity, while being actively inhibited

during the inspiratory phase, have been demonstrated and referred to by Onimaru and Homma as pre-inspiratory (pre-I) cells (Onimaru and Homma, 2003). The late-E activity immediately precedes the inspiratory activity, whereas the post-I activity is also often referred to as stage1-E or early-E activity. The rhythmic *Math1*$^+$ neuron and Onimaru and Homma's pre-I cells are both expiratory and could both be inhibited by the same putative population during inspiration, and possibly belong to the same population of neurons that is respiratory rhythm modulated and that coordinates the pattern of inspiration and expiration.

Most of the *Math1*$^+$ neurons (n = 5) did not exhibit any respiratory modulation during intracellular recordings. These neurons were located closer to the ventral border of the VRC and most likely comprise the *Math1* population contiguous with the RTN, and that gives rise to the chemosensitive *Phox2b*$^+$ population. If so, the non-rhythmic *Math1*$^+$ neurons (which we recorded) are most likely glutamatergic neurons that provide excitatory drive to the respiratory system but do not themselves comprise the inspiratory or the expiratory oscillators (Rose et al., 2009a; Rose et al., 2009b).

Based on initial findings reported here and at recent conferences (Tupal et al., 2011; Tupal et al., 2012), we propose a respiratory network model, wherein the *Math1*$^+$ population is involved in coordinating the phases of the respiratory activity (Fig. 3.6). *Dbx1*$^+$ neurons generate the inspiratory activity in the preBötC (see Chapter 2) whereas the pFRG is the source of expiratory activity. Between cycles of XII output, the rhythmic *Math1*$^+$ neuron (n=1) provides tonic excitatory input to the pFRG, as well as to a population of neurons that then send inhibitory connections to the rhythmogenic neurons in the preBötC, thus delaying the onset of inspiration to preserve the proper phase relationship of the respiratory output. The rhythmogenic preBötC neurons (*Dbx1*$^+$) generate the inspiratory burst (reflected by the XII output) and send excitatory input to a

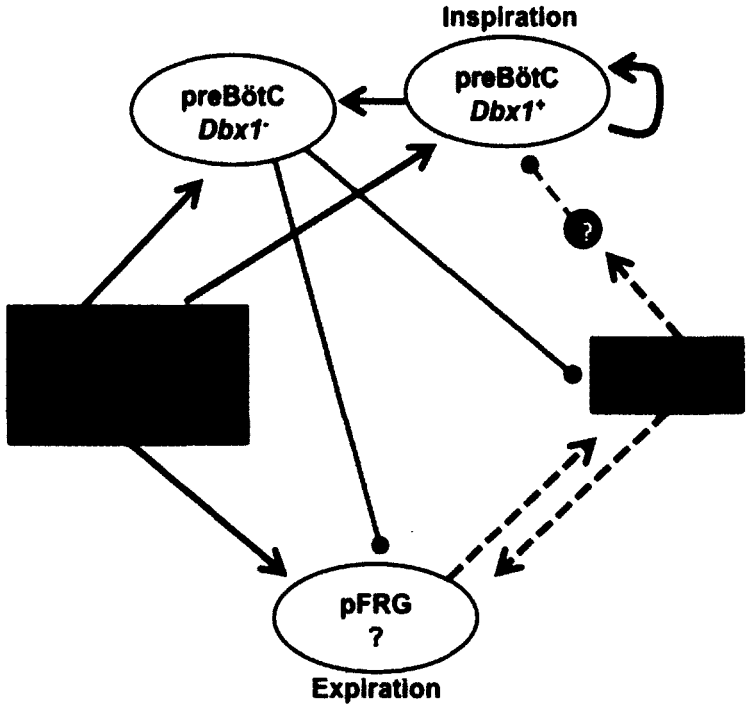

Figure 3.6 Proposed respiratory network consists of two oscillators, for inspiration and expiration. Blue arrows are excitatory connections, red segments are inhibitory connections. The preBötC drives inspiration, while a putative oscillator that drives expiration is indicated as pFRG. The *Math1*$^+$ neuron (n=1) is separate from the *Math1*$^+$ population (n=5) found in the RTN. The preBötC *Dbx1*$^+$ neurons generate the inspiratory burst, and excite other rhythmogenic *Dbx1*$^+$ neurons as well as a separate putative population (*Dbx1*$^-$) that inhibits the expiratory oscillator and the rhythmic *Math1*$^+$ neuron. The rhythmic *Math1*$^+$ neuron (n=1) excites the expiratory oscillator as well as another separate putative population that inhibits the rhytmogenic preBötC neurons. Chemosensitive *Math1*$^+$ and *Phox2b*$^+$ populations in the RTN sense blood $C0_2$ levels and send tonic excitatory inputs to the preBötC and the pFRG.

putative population of neurons that then inhibit the pFRG and the rhythmic *Math1*$^+$ neuron. The rhythmic *Math1*$^+$ neuron exhibit hyperpolarizations that coincide with the XII motor output, which reflect paucisynaptic inhibitory modulation from activity originating in the preBötC. Since the *Math1*$^+$ neurons do not reside in, or comprise the preBötC *per se*, the inhibitory projection neurons could have their soma location anywhere in the VRC at, or rostral to, the preBötC. We propose that the population that inhibits pFRG and the rhythmic *Math1*$^+$ neuron are glycinergic *Dbx1*$^-$ neurons in the preBötC (see Chapter 2). The *Dbx1*$^-$ neurons have projections that extend deeper in the parasagittal plane as well

as axons that project rostrally, and thus may be involved in modulating rostral nuclei such as the RTN/pFRG. In addition, the inspiratory bursts of *Dbx1*$^{-}$ neurons may provide a mimic of preBötC activity to inhibit the pFRG and the rhythmic *Math1*$^{+}$ neuron, making the *Dbx1*$^{-}$ neurons suitable candidates for this putative intervening inhibitory population. Another possibility is that there is a separate inhibitory population intercalated between the preBötC and the pFRG that receives excitatory input from the preBötC and thus inhibit the pFRG and the rhythmic *Math1*$^{+}$ neuron.

Our initial results show that the intrinsic membrane properties, tau_M, R_N, and C_M, of the respiratory modulated *Math1*$^{+}$ neuron are comparable to the non-respiratory neurons. Even though we are not certain if there is a significant difference in the morphological measurements between the two groups, the trend was that the rhythmic *Math1*$^{+}$ neuron exhibited a larger morphology, in soma size and dendritic span, which could be indicative that rhythmic and non-rhythmic *Math1*$^{+}$ neurons may be differentiable on the basis of morphology, as well as physiology. Although further investigations are still necessary to evaluate our hypothesis, the data thus far are promising and consistent with a model in which the *Math1*$^{+}$ population could be important in coordinating the inspiratory and expiratory phases in respiration.

SUMMARY

We evaluated the roles of two genetically defined populations in the neural network underlying respiratory behavior. The work presented in this dissertation improves our understanding of the cellular and ionic bases of respiratory rhythm and pattern generation.

Chapter 2 investigated the rhythmogenic role of the *Dbx1*$^+$ neurons in the preBötC. We characterized the cellular properties including intrinsic membrane properties and morphological properties of *Dbx1*$^+$ neurons to help unravel the cellular mechanisms of respiratory rhythmogenesis. We showed that *Dbx1*$^+$ neurons possess membrane properties consistent with rhythm generation, such as larger drive potential and longer burst latency, combined with the expression of I_{CAN} and disparate expression of I_A and I_h. The rhythmogenic properties of *Dbx1*$^+$ neurons can be attributed to intrinsic excitability that allows temporal summation of incoming excitatory synaptic inputs necessary for generating robust inspiratory bursts. Furthermore, the dendritic morphology and axonal projection patterns of *Dbx1*$^+$ neurons suggest that they are specialized for integrating local synaptic inputs from other *Dbx1*$^+$ neurons and sending output to neighboring *Dbx1*$^+$ neurons, which could be important for initiating and maintaining bursts and synchronizing activity during the inspiratory phase.

In Chapter 3, we examined the potential role of *Math1*$^+$ neurons in coordinating the respiratory pattern. *Math1*$^+$ neurons have been shown to influence the temporal relationship of the inspiratory and expiratory outputs (Tupal et al., 2011; Tupal et al., 2012). We observed expiratory activity in one of the six *Math1*$^+$ neurons, and then performed a comparative physiological and morphological characterization between the respiratory and the non-respiratory modulated neurons. Although the measured intrinsic properties were identical between the two groups, the morphology differed between the

rhythmic and the non-rhythmic *Math1*$^+$ neurons. The larger morphological span and rhythmic expiratory modulation might suggest a function in coordinating inspiratory and expiratory phases. We propose a respiratory network where *Math1*$^+$ neurons plays an important role in coordinating the inspiratory output from the preBötC and the expiratory output from the pFRG. Although, further evaluation is necessary, our data on *Math1*$^+$ neurons are thus far suggestive of a role in coordinating the pattern of respiratory rhythm.

In summary, we identified and characterized hindbrain interneurons according to their developmental lineages. We characterized their physiological and morphological properties to provide further knowledge in elucidating the cellular mechanisms underlying the generation and coordination of the respiratory rhythm.

REFERENCES

Abbott SB, Stornetta RL, Coates MB, Guyenet PG (2011) Phox2b-expressing neurons of the parafacial region regulate breathing rate, inspiration, and expiration in conscious rats. J Neurosci 31:16410-16422.

Acker CD, White JA (2007) Roles of IA and morphology in action potential propagation in CA1 pyramidal cell dendrites. J Comput Neurosci 23:201-216.

Al-Mosawie A, Wilson JM, Brownstone RM (2007) Heterogeneity of V2-derived interneurons in the adult mouse spinal cord. Eur J Neurosci 26:3003-3015.

Alvarez FJ, Jonas PC, Sapir T, Hartley R, Berrocal MC, Geiman EJ, Todd AJ, Goulding M (2005) Postnatal phenotype and localization of spinal cord V1 derived interneurons. J Comp Neurol 493:177-192.

Arber S, Han B, Mendelsohn M, Smith M, Jessell TM, Sockanathan S (1999) Requirement for the homeobox gene Hb9 in the consolidation of motor neuron identity. Neuron 23:659-674.

Arimura N, Kaibuchi K (2007) Neuronal polarity: from extracellular signals to intracellular mechanisms. Nat Rev Neurosci 8:194-205.

Ben-Arie N, Bellen HJ, Armstrong DL, McCall AE, Gordadze PR, Guo Q, Matzuk MM, Zoghbi HY (1997) Math1 is essential for genesis of cerebellar granule neurons. Nature 390:169-172.

Bermingham NA, Hassan BA, Wang VY, Fernandez M, Banfi S, Bellen HJ, Fritzsch B, Zoghbi HY (2001) Proprioceptor pathway development is dependent on Math1. Neuron 30:411-422.

Bianchi AL, Denavit-Saubie M, Champagnat J (1995) Central control of breathing in mammals: neuronal circuitry, membrane properties, and neurotransmitters. Physiol Rev 75:1-45.

Birk OS, Casiano DE, Wassif CA, Cogliati T, Zhao L, Zhao Y, Grinberg A, Huang S, Kreidberg JA, Parker KL, Porter FD, Westphal H (2000) The LIM homeobox gene Lhx9 is essential for mouse gonad formation. Nature 403:909-913.

Blessing WW (1997) The lower brainstem and bodily homeostasis. New York: Oxford University Press.

Bouvier J, Thoby-Brisson M, Renier N, Dubreuil V, Ericson J, Champagnat J, Pierani A, Chedotal A, Fortin G (2010) Hindbrain interneurons and axon guidance signaling critical for breathing. Nat Neurosci 13:1066-1074.

Briscoe J, Ericson J (2001) Specification of neuronal fates in the ventral neural tube. Curr Opin Neurobiol 11:43-49.

Briscoe J, Sussel L, Serup P, Hartigan-O'Connor D, Jessell TM, Rubenstein JL, Ericson J (1999) Homeobox gene Nkx2.2 and specification of neuronal identity by graded Sonic hedgehog signalling. Nature 398:622-627.

Brockhaus J, Ballanyi K (1998) Synaptic inhibition in the isolated respiratory network of neonatal rats. Eur J Neurosci 10:3823-3839.

Brown AG (1981) Organization in the spinal cord : the anatomy and physiology of identified neurones. Berlin ; New York: Springer-Verlag.

Burrill JD, Moran L, Goulding MD, Saueressig H (1997) PAX2 is expressed in multiple spinal cord interneurons, including a population of EN1+ interneurons that require PAX6 for their development. Development 124:4493-4503.

Causeret F, Ensini M, Teissier A, Kessaris N, Richardson WD, Lucas de Couville T, Pierani A (2011) Dbx1-expressing cells are necessary for the survival of the mammalian anterior neural and craniofacial structures. PLoS One 6:e19367.

Cheng L, Samad OA, Xu Y, Mizuguchi R, Luo P, Shirasawa S, Goulding M, Ma Q (2005) Lbx1 and Tlx3 are opposing switches in determining GABAergic versus glutamatergic transmitter phenotypes. Nat Neurosci 8:1510-1515.

Cheng L, Arata A, Mizuguchi R, Qian Y, Karunaratne A, Gray PA, Arata S, Shirasawa S, Bouchard M, Luo P, Chen CL, Busslinger M, Goulding M, Onimaru H, Ma Q (2004) Tlx3 and Tlx1 are post-mitotic selector genes determining glutamatergic over GABAergic cell fates. Nat Neurosci 7:510-517.

Crone SA, Zhong G, Harris-Warrick R, Sharma K (2009) In mice lacking V2a interneurons, gait depends on speed of locomotion. J Neurosci 29:7098-7109.

Crone SA, Quinlan KA, Zagoraiou L, Droho S, Restrepo CE, Lundfald L, Endo T, Setlak J, Jessell TM, Kiehn O, Sharma K (2008) Genetic ablation of V2a ipsilateral interneurons disrupts left-right locomotor coordination in mammalian spinal cord. Neuron 60:70-83.

Crowder EA, Saha MS, Pace RW, Zhang H, Prestwich GD, Del Negro CA (2007) Phosphatidylinositol 4,5-bisphosphate regulates inspiratory burst activity in the neonatal mouse preBotzinger complex. J Physiol 582:1047-1058.

Dasen JS, Tice BC, Brenner-Morton S, Jessell TM (2005) A Hox regulatory network establishes motor neuron pool identity and target-muscle connectivity. Cell 123:477-491.

de Anda FC, Pollarolo G, Da Silva JS, Camoletto PG, Feiguin F, Dotti CG (2005) Centrosome localization determines neuronal polarity. Nature 436:704-708.

Del Negro CA, Morgado-Valle C, Feldman JL (2002a) Respiratory rhythm: an emergent network property? Neuron 34:821-830.

Del Negro CA, Koshiya N, Butera RJ, Jr., Smith JC (2002b) Persistent sodium current, membrane properties and bursting behavior of pre-Bötzinger complex inspiratory neurons in vitro. J Neurophysiol 88:2242-2250.

Del Negro CA, Kam K, Hayes JA, Feldman JL (2009) Asymmetric control of inspiratory and expiratory phases by excitability in the respiratory network of neonatal mice in vitro. J Physiol 587:1217-1231.

Del Negro CA, Morgado-Valle C, Hayes JA, Mackay DD, Pace RW, Crowder EA, Feldman JL (2005) Sodium and calcium current-mediated pacemaker neurons and respiratory rhythm generation. J Neurosci 25:446-453.

Dobbins EG, Feldman JL (1994) Brainstem network controlling descending drive to phrenic motoneurons in rat. J Comp Neurol 347:64-86.

Dougherty KJ, Kiehn O (2010) Firing and cellular properties of V2a interneurons in the rodent spinal cord. J Neurosci 30:24-37.

Dubreuil V, Hirsch MR, Pattyn A, Brunet JF, Goridis C (2000) The Phox2b transcription factor coordinately regulates neuronal cell cycle exit and identity. Development 127:5191-5201.

Dubreuil V, Ramanantsoa N, Trochet D, Vaubourg V, Amiel J, Gallego J, Brunet JF, Goridis C (2008) A human mutation in Phox2b causes lack of CO2

chemosensitivity, fatal central apnea, and specific loss of parafacial neurons. Proc Natl Acad Sci U S A 105:1067-1072.

Dunmyre JR, Del Negro CA, Rubin JE (2011) Interactions of persistent sodium and calcium-activated nonspecific cationic currents yield dynamically distinct bursting regimes in a model of respiratory neurons. J Comput Neurosci.

Ellenberger HH, Feldman JL (1990) Subnuclear organization of the lateral tegmental field of the rat. I: Nucleus ambiguus and ventral respiratory group. J Comp Neurol 294:202-211.

Elsen FP, Ramirez JM (2005) Postnatal development differentially affects voltage-activated calcium currents in respiratory rhythmic versus nonrhythmic neurons of the pre-Botzinger complex. J Neurophysiol 94:1423-1431.

Ericson J, Rashbass P, Schedl A, Brenner-Morton S, Kawakami A, van Heyningen V, Jessell TM, Briscoe J (1997) Pax6 controls progenitor cell identity and neuronal fate in response to graded Shh signaling. Cell 90:169-180.

Esch T, Lemmon V, Banker G (1999) Local presentation of substrate molecules directs axon specification by cultured hippocampal neurons. J Neurosci 19:6417-6426.

Ezure K (1990) Synaptic connections between medullary respiratory neurons and considerations on the genesis of respiratory rhythm. Prog Neurobiol 35:429-450.

Feldman JL, Smith JC (1989) Cellular mechanisms underlying modulation of breathing pattern in mammals. Ann N Y Acad Sci 563:114-130.

Feldman JL, Del Negro CA (2006) Looking for inspiration: new perspectives on respiratory rhythm. Nat Rev Neurosci 7:232-242.

Funk GD, Smith JC, Feldman JL (1993) Generation and transmission of respiratory oscillations in medullary slices: role of excitatory amino acids. J Neurophysiol 70:1497-1515.

Garcia-Campmany L, Stam FJ, Goulding M (2010) From circuits to behaviour: motor networks in vertebrates. Curr Opin Neurobiol 20:116-125.

Goridis C, Dubreuil V, Thoby-Brisson M, Fortin G, Brunet JF (2010) Phox2b, congenital central hypoventilation syndrome and the control of respiration. Semin Cell Dev Biol.

Gosgnach S, Lanuza GM, Butt SJ, Saueressig H, Zhang Y, Velasquez T, Riethmacher D, Callaway EM, Kiehn O, Goulding M (2006) V1 spinal neurons regulate the speed of vertebrate locomotor outputs. Nature 440:215-219.

Goulding M (2009) Circuits controlling vertebrate locomotion: moving in a new direction. Nat Rev Neurosci 10:507-518.

Goulding M, Pfaff SL (2005) Development of circuits that generate simple rhythmic behaviors in vertebrates. Curr Opin Neurobiol 15:14-20.

Goulding M, Lanuza G, Sapir T, Narayan S (2002) The formation of sensorimotor circuits. Curr Opin Neurobiol 12:508-515.

Gray PA (2008) Transcription factors and the genetic organization of brain stem respiratory neurons. J Appl Physiol 104:1513-1521.

Gray PA, Rekling JC, Bocchiaro CM, Feldman JL (1999) Modulation of respiratory frequency by peptidergic input to rhythmogenic neurons in the preBötzinger complex. Science 286:1566-1568.

Gray PA, Janczewski WA, Mellen N, McCrimmon DR, Feldman JL (2001) Normal breathing requires preBötzinger complex neurokinin-1 receptor-expressing neurons. Nat Neurosci 4:927-930.

Gray PA, Hayes JA, Ling G, Llona I, Tupai S, Picardo MC, Ross S, Hirata T, Corbin JG, Eugenin J, Del Negro CA (2010) Developmental Origin of preBötzinger Complex Respiratory Neurons. J Neurosci 30:14883-14895.

Gray PA et al. (2004) Mouse brain organization revealed through direct genome-scale TF expression analysis. Science 306:2255-2257.

Greer JJ, Smith JC, Feldman JL (1991) Role of excitatory amino acids in the generation and transmission of respiratory drive in neonatal rat. J Physiol 437:727-749.

Grillner S (2006) Biological pattern generation: the cellular and computational logic of networks in motion. Neuron 52:751-766.

Gross MK, Dottori M, Goulding M (2002) Lbx1 specifies somatosensory association interneurons in the dorsal spinal cord. Neuron 34:535-549.

Gulledge AT, Kampa BM, Stuart GJ (2005) Synaptic integration in dendritic trees. J Neurobiol 64:75-90.

Guyenet PG, Wang H (2001) Pre-Bötzinger neurons with preinspiratory discharges "in vivo" express NK1 receptors in the rat. J Neurophysiol 86:438-446.

Guyenet PG, Sevigny CP, Weston MC, Stornetta RL (2002) Neurokinin-1 receptor-expressing cells of the ventral respiratory group are functionally heterogeneous and predominantly glutamatergic. J Neurosci 22:3806-3816.

Guyenet PG, Bayliss DA, Stornetta RL, Fortuna MG, Abbott SB, DePuy SD (2009) Retrotrapezoid nucleus, respiratory chemosensitivity and breathing automaticity. Respir Physiol Neurobiol 168:59-68.

Hayes JA (2007) Phenotypic properties and intrinsic currents of neurons involved in the neural generation of mammalian breathing. In: Applied Science, p 153. Williamsburg, Virginia: The College of William and Mary.

Hayes JA, Del Negro CA (2007) Neurokinin Receptor-Expressing PreBötzinger Complex Neurons in Neonatal Mice Studied In Vitro. J Neurophysiol 97:4215-4224.

Helms AW, Johnson JE (2003) Specification of dorsal spinal cord interneurons. Curr Opin Neurobiol 13:42-49.

Higashijima S, Masino MA, Mandel G, Fetcho JR (2004) Engrailed-1 expression marks a primitive class of inhibitory spinal interneuron. J Neurosci 24:5827-5839.

Hirata T, Li P, Lanuza GM, Cocas LA, Huntsman MM, Corbin JG (2009) Identification of distinct telencephalic progenitor pools for neuronal diversity in the amygdala. Nat Neurosci 12:141-149.

Hoffman DA, Magee JC, Colbert CM, Johnston D (1997) K+ channel regulation of signal propagation in dendrites of hippocampal pyramidal neurons. Nature 387:869-875.

Jacobson C, Schnapp B, Banker GA (2006) A change in the selective translocation of the Kinesin-1 motor domain marks the initial specification of the axon. Neuron 49:797-804.

Janczewski WA, Feldman JL (2006) Distinct rhythm generators for inspiration and expiration in the juvenile rat. J Physiol 570:407-420.

Jessell TM (2000) Neuronal specification in the spinal cord: inductive signals and transcriptional codes. Nat Rev Genet 1:20-29.

Karunaratne A, Hargrave M, Poh A, Yamada T (2002) GATA proteins identify a novel ventral interneuron subclass in the developing chick spinal cord. Dev Biol 249:30-43.

Kiehn O (2006) Locomotor circuits in the mammalian spinal cord. Annu Rev Neurosci 29:279-306.

Kiehn O (2011) Development and functional organization of spinal locomotor circuits. Current opinion in neurobiology 21:100-109.

Kim EJ, Battiste J, Nakagawa Y, Johnson JE (2008) Ascl1 (Mash1) lineage cells contribute to discrete cell populations in CNS architecture. Mol Cell Neurosci 38:595-606.

Kjaerulff O, Kiehn O (1996) Distribution of networks generating and coordinating locomotor activity in the neonatal rat spinal cord in vitro: a lesion study. J Neurosci 16:5777-5794.

Koizumi H, Smith JC (2008) Persistent Na+ and K+-dominated leak currents contribute to respiratory rhythm generation in the pre-Bötzinger complex in vitro. J Neurosci 28:1773-1785.

Koizumi H, Wilson CG, Wong S, Yamanishi T, Koshiya N, Smith JC (2008) Functional imaging, spatial reconstruction, and biophysical analysis of a respiratory motor circuit isolated in vitro. J Neurosci 28:2353-2365.

Koshiya N, Smith JC (1999) Neuronal pacemaker for breathing visualized in vitro. Nature 400:360-363.

Krey RA, Goodreau AM, Arnold TB, Del Negro CA (2010) Outward Currents Contributing to Inspiratory Burst Termination in preBotzinger Complex Neurons of Neonatal Mice Studied in Vitro. Front Neural Circuits 4:124.

Lanuza GM, Gosgnach S, Pierani A, Jessell TM, Goulding M (2004) Genetic identification of spinal interneurons that coordinate left-right locomotor activity necessary for walking movements. Neuron 42:375-386.

Lee KJ, Jessell TM (1999) The specification of dorsal cell fates in the vertebrate central nervous system. Annu Rev Neurosci 22:261-294.

Liem KF, Jr., Jessell TM, Briscoe J (2000) Regulation of the neural patterning activity of sonic hedgehog by secreted BMP inhibitors expressed by notochord and somites. Development 127:4855-4866.

Llinas RR (1988) The intrinsic electrophysiological properties of mammalian neurons: insights into central nervous system function. Science 242:1654-1664.

Lu S, Bogarad LD, Murtha MT, Ruddle FH (1992) Expression pattern of a murine homeobox gene, Dbx, displays extreme spatial restriction in embryonic forebrain and spinal cord. Proc Natl Acad Sci U S A 89:8053-8057.

Lundfald L, Restrepo CE, Butt SJ, Peng CY, Droho S, Endo T, Zeilhofer HU, Sharma K, Kiehn O (2007) Phenotype of V2-derived interneurons and their relationship to the axon guidance molecule EphA4 in the developing mouse spinal cord. Eur J Neurosci 26:2989-3002.

Machold R, Fishell G (2005) Math1 is expressed in temporally discrete pools of cerebellar rhombic-lip neural progenitors. Neuron 48:17-24.

Madisen L, Zwingman TA, Sunkin SM, Oh SW, Zariwala HA, Gu H, Ng LL, Palmiter RD, Hawrylycz MJ, Jones AR, Lein ES, Zeng H (2010) A robust and high-throughput Cre reporting and characterization system for the whole mouse brain. Nat Neurosci 13:133-140.

Magee JC (1999) Dendritic Ih normalizes temporal summation in hippocampal CA1 neurons. Nat Neurosci 2:508-514.

Magee JC (2000) Dendritic integration of excitatory synaptic input. Nat Rev Neurosci 1:181-190.

Mainen ZF, Sejnowski TJ (1996) Influence of dendritic structure on firing pattern in model neocortical neurons. Nature 382:363-366.

Masland RH (2004) Neuronal cell types. Curr Biol 14:R497-500.

Matise MP, Joyner AL (1997) Expression patterns of developmental control genes in normal and Engrailed-1 mutant mouse spinal cord reveal early diversity in developing interneurons. J Neurosci 17:7805-7816.

McKay LC, Janczewski WA, Feldman JL (2005) Sleep-disordered breathing after targeted ablation of preBotzinger complex neurons. Nat Neurosci 8:1142-1144.

Mellen NM, Janczewski WA, Bocchiaro CM, Feldman JL (2003) Opioid-induced quantal slowing reveals dual networks for respiratory rhythm generation. Neuron 37:821-826.

Migliore M, Messineo L, Ferrante M (2004) Dendritic Ih selectively blocks temporal summation of unsynchronized distal inputs in CA1 pyramidal neurons. J Comput Neurosci 16:5-13.

Moran-Rivard L, Kagawa T, Saueressig H, Gross MK, Burrill J, Goulding M (2001) Evx1 is a postmitotic determinant of v0 interneuron identity in the spinal cord. Neuron 29:385-399.

Morgado-Valle C, Baca SM, Feldman JL (2010) Glycinergic Pacemaker Neurons in PreBötzinger Complex of Neonatal Mouse. J Neurosci 30:3634-3639.

Muller T, Brohmann H, Pierani A, Heppenstall PA, Lewin GR, Jessell TM, Birchmeier C (2002) The homeodomain factor lbx1 distinguishes two major programs of neuronal differentiation in the dorsal spinal cord. Neuron 34:551-562.

Myatt DR, Hadlington T, Ascoli GA, Nasuto SJ (2012) Neuromantic - from semi-manual to semi-automatic reconstruction of neuron morphology. Front Neuroinform 6:4.

Nattie E, Li A (2006) Neurokinin-1 receptor-expressing neurons in the ventral medulla are essential for normal central and peripheral chemoreception in the conscious rat. J Appl Physiol 101:1596-1606.

Onimaru H, Homma I (2003) A novel functional neuron group for respiratory rhythm generation in the ventral medulla. J Neurosci 23:1478-1486.

Onimaru H, Ballanyi K, Homma I (2003) Contribution of Ca2+-dependent conductances to membrane potential fluctuations of medullary respiratory neurons of newborn rats in vitro. J Physiol 552:727-741.

Onimaru H, Ikeda K, Kawakami K (2008) CO2-sensitive preinspiratory neurons of the parafacial respiratory group express Phox2b in the neonatal rat. J Neurosci 28:12845-12850.

Onimaru H, Ikeda K, Kawakami K (2012) Postsynaptic mechanisms of CO(2) responses in parafacial respiratory neurons of newborn rats. J Physiol 590:1615-1624.

Orlovsky GN, Deliagina TG, Grillner S (1999) Neuronal control of locomotion : from mollusc to man. New York: Oxford University Press.

Pace RW, Mackay DD, Feldman JL, Del Negro CA (2007a) Inspiratory bursts in the preBötzinger Complex depend on a calcium-activated nonspecific cationic current linked to glutamate receptors. J Physiol 582:113-125.

Pace RW, Mackay DD, Feldman JL, Del Negro CA (2007b) Role of persistent sodium current in mouse preBotzinger Complex neurons and respiratory rhythm generation. J Physiol 580:485-496.

Pagliardini S, Adachi T, Ren J, Funk GD, Greer JJ (2005) Fluorescent tagging of rhythmically active respiratory neurons within the pre-Bötzinger complex of rat medullary slice preparations. J Neurosci 25:2591-2596.

Pagliardini S, Janczewski WA, Tan W, Dickson CT, Deisseroth K, Feldman JL (2011) Active expiration induced by excitation of ventral medulla in adult anesthetized rats. J Neurosci 31:2895-2905.

Pagliardini S, Ren J, Gray PA, Vandunk C, Gross M, Goulding M, Greer JJ (2008) Central respiratory rhythmogenesis is abnormal in lbx1- deficient mice. J Neurosci 28:11030-11041.

Pattyn A, Hirsch M, Goridis C, Brunet JF (2000) Control of hindbrain motor neuron differentiation by the homeobox gene Phox2b. Development 127:1349-1358.

Pattyn A, Morin X, Cremer H, Goridis C, Brunet JF (1997) Expression and interactions of the two closely related homeobox genes Phox2a and Phox2b during neurogenesis. Development 124:4065-4075.

Pattyn A, Simplicio N, van Doorninck JH, Goridis C, Guillemot F, Brunet JF (2004) Ascl1/ Mash1 is required for the development of central serotonergic neurons. Nat Neurosci 7:589-595.

Pena F, Parkis MA, Tryba AK, Ramirez JM (2004) Differential Contribution of Pacemaker Properties to the Generation of Respiratory Rhythms during Normoxia and Hypoxia. Neuron 43:105-117.

Peng CY, Yajima H, Burns CE, Zon LI, Sisodia SS, Pfaff SL, Sharma K (2007) Notch and MAML signaling drives Scl-dependent interneuron diversity in the spinal cord. Neuron 53:813-827.

Pfaff SL, Mendelsohn M, Stewart CL, Edlund T, Jessell TM (1996) Requirement for LIM homeobox gene Isl1 in motor neuron generation reveals a motor neuron-dependent step in interneuron differentiation. Cell 84:309-320.

Pierani A, Brenner-Morton S, Chiang C, Jessell TM (1999) A sonic hedgehog-independent, retinoid-activated pathway of neurogenesis in the ventral spinal cord. Cell 97:903-915.

Pierani A, Moran-Rivard L, Sunshine MJ, Littman DR, Goulding M, Jessell TM (2001) Control of interneuron fate in the developing spinal cord by the progenitor homeodomain protein Dbx1. Neuron 29:367-384.

Porter FD, Drago J, Xu Y, Cheema SS, Wassif C, Huang SP, Lee E, Grinberg A, Massalas JS, Bodine D, Alt F, Westphal H (1997) Lhx2, a LIM homeobox gene, is required for eye, forebrain, and definitive erythrocyte development. Development 124:2935-2944.

Pratt CA, Jordan LM (1987) Ia inhibitory interneurons and Renshaw cells as contributors to the spinal mechanisms of fictive locomotion. J Neurophysiol 57:56-71.

Ptak K, Zummo GG, Alheid GF, Tkatch T, Surmeier DJ, McCrimmon DR (2005) Sodium currents in medullary neurons isolated from the pre-Bötzinger complex region. J Neurosci 25:5159-5170.

Qian Y, Shirasawa S, Chen CL, Cheng L, Ma Q (2002) Proper development of relay somatic sensory neurons and D2/D4 interneurons requires homeobox genes Rnx/Tlx-3 and Tlx-1. Genes Dev 16:1220-1233.

Rall W, Agon-Snir H (1998) Cable Theory for Dendritic Neurons. In: Methods in neuronal modeling : from ions to networks, 2nd Edition (Koch C, Segev I, eds), pp 27-92. Cambridge, Mass.: MIT Press.

Ramanantsoa N, Hirsch MR, Thoby-Brisson M, Dubreuil V, Bouvier J, Ruffault PL, Matrot B, Fortin G, Brunet JF, Gallego J, Goridis C (2011) Breathing without CO2 Chemosensitivity in Conditional Phox2b Mutants. J Neurosci 31:12880-12888.

Ramirez JM, Viemari JC (2005) Determinants of inspiratory activity. Respir Physiol Neurobiol 147:145-157.

Rekling JC, Feldman JL (1998) PreBötzinger complex and pacemaker neurons: hypothesized site and kernel for respiratory rhythm generation. Annu Rev Physiol 60:385-405.

Rekling JC, Champagnat J, Denavit-Saubie M (1996a) Thyrotropin-releasing hormone (TRH) depolarizes a subset of inspiratory neurons in the newborn mouse brain stem in vitro. J Neurophysiol 75:811-819.

Rekling JC, Champagnat J, Denavit-Saubie M (1996b) Electroresponsive properties and membrane potential trajectories of three types of inspiratory neurons in the newborn mouse brain stem in vitro. J Neurophysiol 75:795-810.

Ren J, Poon BY, Tang Y, Funk GD, Greer JJ (2006) Ampakines alleviate respiratory depression in rats. Am J Respir Crit Care Med 174:1384-1391.

Richter DW (1982) Generation and maintenance of the respiratory rhythm. J Exp Biol 100:93-107.

Richter DW, Spyer KM (2001) Studying rhythmogenesis of breathing: comparison of in vivo and in vitro models. Trends Neurosci 24:464-472.

Ritter B, Zhang W (2000) Early postnatal maturation of GABAA-mediated inhibition in the brainstem respiratory rhythm-generating network of the mouse. Eur J Neurosci 12:2975-2984.

Rose MF, Ahmad KA, Thaller C, Zoghbi HY (2009a) Excitatory neurons of the proprioceptive, interoceptive, and arousal hindbrain networks share a developmental requirement for Math1. Proc Natl Acad Sci U S A 106:22462-22467.

Rose MF, Ren J, Ahmad KA, Chao HT, Klisch TJ, Flora A, Greer JJ, Zoghbi HY (2009b) Math1 is essential for the development of hindbrain neurons critical for perinatal breathing. Neuron 64:341-354.

Rubin JE, Hayes JA, Mendenhall JL, Del Negro CA (2009) Calcium-activated nonspecific cation current and synaptic depression promote network-dependent burst oscillations. Proc Natl Acad Sci U S A 106:2939-2944.

Sapir T, Geiman EJ, Wang Z, Velasquez T, Mitsui S, Yoshihara Y, Frank E, Alvarez FJ, Goulding M (2004) Pax6 and engrailed 1 regulate two distinct aspects of renshaw cell development. J Neurosci 24:1255-1264.

Saueressig H, Burrill J, Goulding M (1999) Engrailed-1 and netrin-1 regulate axon pathfinding by association interneurons that project to motor neurons. Development 126:4201-4212.

Schwarzacher SW, Smith JC, Richter DW (1995) Pre-Bötzinger complex in the cat. J Neurophysiol 73:1452-1461.

Schwarzacher SW, Rub U, Deller T (2010) Neuroanatomical characteristics of the human pre-Botzinger complex and its involvement in neurodegenerative brainstem diseases. Brain.

Scorcioni R, Polavaram S, Ascoli GA (2008) L-Measure: a web-accessible tool for the analysis, comparison and search of digital reconstructions of neuronal morphologies. Nat Protoc 3:866-876.

Shao XM, Feldman JL (1997) Respiratory rhythm generation and synaptic inhibition of expiratory neurons in pre-Botzinger complex: differential roles of glycinergic and GABAergic neural transmission. J Neurophysiol 77:1853-1860.

Shelly M, Lim BK, Cancedda L, Heilshorn SC, Gao H, Poo MM (2010) Local and long-range reciprocal regulation of cAMP and cGMP in axon/dendrite formation. Science 327:547-552.

Shirasaki R, Pfaff SL (2002) Transcriptional codes and the control of neuronal identity. Annu Rev Neurosci 25:251-281.

Shoji H, Ito T, Wakamatsu Y, Hayasaka N, Ohsaki K, Oyanagi M, Kominami R, Kondoh H, Takahashi N (1996) Regionalized expression of the Dbx family homeobox genes in the embryonic CNS of the mouse. Mech Dev 56:25-39.

Sieber MA, Storm R, Martinez-de-la-Torre M, Muller T, Wende H, Reuter K, Vasyutina E, Birchmeier C (2007) Lbx1 acts as a selector gene in the fate determination of somatosensory and viscerosensory relay neurons in the hindbrain. J Neurosci 27:4902-4909.

Smith E, Hargrave M, Yamada T, Begley CG, Little MH (2002) Coexpression of SCL and GATA3 in the V2 interneurons of the developing mouse spinal cord. Dev Dyn 224:231-237.

Smith JC, Morrison DE, Ellenberger HH, Otto MR, Feldman JL (1989) Brainstem projections to the major respiratory neuron populations in the medulla of the cat. J Comp Neurol 281:69-96.

Smith JC, Ellenberger HH, Ballanyi K, Richter DW, Feldman JL (1991) Pre-Bötzinger complex: a brainstem region that may generate respiratory rhythm in mammals. Science 254:726-729.

Stornetta RL, Rosin DL, Wang H, Sevigny CP, Weston MC, Guyenet PG (2003) A group of glutamatergic interneurons expressing high levels of both neurokinin-1 receptors and somatostatin identifies the region of the pre-Bötzinger complex. J Comp Neurol 455:499-512.

Stornetta RL, Moreira TS, Takakura AC, Kang BJ, Chang DA, West GH, Brunet JF, Mulkey DK, Bayliss DA, Guyenet PG (2006) Expression of Phox2b by brainstem neurons involved in chemosensory integration in the adult rat. J Neurosci 26:10305-10314.

Sugino K, Hempel CM, Miller MN, Hattox AM, Shapiro P, Wu C, Huang ZJ, Nelson SB (2006) Molecular taxonomy of major neuronal classes in the adult mouse forebrain. Nat Neurosci 9:99-107.

Takakura AC, Moreira TS, Stornetta RL, West GH, Gwilt JM, Guyenet PG (2008) Selective lesion of retrotrapezoid Phox2b-expressing neurons raises the apnoeic threshold in rats. J Physiol 586:2975-2991.

Tan W, Janczewski WA, Yang P, Shao XM, Callaway EM, Feldman JL (2008) Silencing preBötzinger Complex somatostatin-expressing neurons induces persistent apnea in awake rat. Nat Neurosci 11:538-540.

Tanabe Y, Jessell TM (1996) Diversity and pattern in the developing spinal cord. Science 274:1115-1123.

Thoby-Brisson M, Ramirez JM (2001) Identification of two types of inspiratory pacemaker neurons in the isolated respiratory neural network of mice. J Neurophysiol 86:104-112.

Thoby-Brisson M, Telgkamp P, Ramirez JM (2000) The role of the hyperpolarization-activated current in modulating rhythmic activity in the isolated respiratory network of mice. J Neurosci 20:2994-3005.

Thoby-Brisson M, Karlen M, Wu N, Charnay P, Champagnat J, Fortin G (2009) Genetic identification of an embryonic parafacial oscillator coupling to the preBotzinger complex. Nat Neurosci 12:1028-1035.

Tupal S, McMurray G, Gray PA (2011) Testing the dual oscillator hypothesis: Effects of Dbx1, Atoh1, or MafB mutation on inspiratory and expiratory output in mice.

Program No. 189.03. In: 2011 Neuroscience Meeting Planner. Washington, DC: Society for Neuroscience.

Tupal S, Wei-Hsiang H, Zoghbi HY, Gray PA (2012) Neural Network Underlying Complex Respiratory Behaviors. A Paper presented In: Cellular and Network Functions in the Spinal Cord Conference. May 22-25, 2012;. University of Wisconsin, Madison, WI.

Volgin DV, Rukhadze I, Kubin L (2008) Hypoglossal premotor neurons of the intermediate medullary reticular region express cholinergic markers. J Appl Physiol 105:1576-1584.

Vue TY, Aaker J, Taniguchi A, Kazemzadeh C, Skidmore JM, Martin DM, Martin JF, Treier M, Nakagawa Y (2007) Characterization of progenitor domains in the developing mouse thalamus. J Comp Neurol 505:73-91.

Wallen-Mackenzie A, Gezelius H, Thoby-Brisson M, Nygard A, Enjin A, Fujiyama F, Fortin G, Kullander K (2006) Vesicular glutamate transporter 2 is required for central respiratory rhythm generation but not for locomotor central pattern generation. J Neurosci 26:12294-12307.

Wang H, Stornetta RL, Rosin DL, Guyenet PG (2001) Neurokinin-1 receptor-immunoreactive neurons of the ventral respiratory group in the rat. J Comp Neurol 434:128-146.

Wang VY, Rose MF, Zoghbi HY (2005) Math1 expression redefines the rhombic lip derivatives and reveals novel lineages within the brainstem and cerebellum. Neuron 48:31-43.

Wenninger JM, Pan LG, Klum L, Leekley T, Bastastic J, Hodges MR, Feroah TR, Davis S, Forster HV (2004) Large lesions in the pre-Bötzinger complex area eliminate eupneic respiratory rhythm in awake goats. J Appl Physiol 97:1629-1636.

Wilson L, Maden M (2005) The mechanisms of dorsoventral patterning in the vertebrate neural tube. Dev Biol 282:1-13.

Winter SM, Fresemann J, Schnell C, Oku Y, Hirrlinger J, Hulsmann S (2009) Glycinergic interneurons are functionally integrated into the inspiratory network of mouse medullary slices. Pflugers Arch 458:459-469.

Yamada M, Terao M, Terashima T, Fujiyama T, Kawaguchi Y, Nabeshima Y, Hoshino M (2007) Origin of climbing fiber neurons and their developmental dependence on Ptf1a. J Neurosci 27:10924-10934.

Zagoraiou L, Akay T, Martin JF, Brownstone RM, Jessell TM, Miles GB (2009) A cluster of cholinergic premotor interneurons modulates mouse locomotor activity. Neuron 64:645-662.

Zavala-Tecuapetla C, Aguileta MA, Lopez-Guerrero JJ, Gonzalez-Marin MC, Pena F (2008) Calcium-activated potassium currents differentially modulate respiratory rhythm generation. Eur J Neurosci 27:2871-2884.

Zhang Y, Narayan S, Geiman E, Lanuza GM, Velasquez T, Shanks B, Akay T, Dyck J, Pearson K, Gosgnach S, Fan CM, Goulding M (2008) V3 spinal neurons establish a robust and balanced locomotor rhythm during walking. Neuron 60:84-96.

Zhong G, Droho S, Crone SA, Dietz S, Kwan AC, Webb WW, Sharma K, Harris-Warrick RM (2010) Electrophysiological characterization of V2a interneurons and their

locomotor-related activity in the neonatal mouse spinal cord. J Neurosci 30:170-182.

Zhou Y, Yamamoto M, Engel JD (2000) GATA2 is required for the generation of V2 interneurons. Development 127:3829-3838.